AGU PUBLICATIONS

Global Biogeochemical Cycles

RESEARCH ARTICLE
10.1002/2014GB005050

Key Points:
- Large-scale data sets of DON and DOP constrain the global model
- Preferential DOP remineralization and uptake stimulate significant N_2 fixation
- The marine fixed nitrogen inventory increases due to non-Redfield DOP cycling

Correspondence to:
C. J. Somes,
csomes@geomar.de

Citation:
Somes, C. J., and A. Oschlies (2015), On the influence of "non-Redfield" dissolved organic nutrient dynamics on the spatial distribution of N_2 fixation and the size of the marine fixed nitrogen inventory, *Global Biogeochem. Cycles*, *29*, 973–993, doi:10.1002/2014GB005050.

Received 2 DEC 2014
Accepted 19 MAY 2015
Accepted article online 25 MAY 2015
Published online 14 JUL 2015

On the influence of "non-Redfield" dissolved organic nutrient dynamics on the spatial distribution of N_2 fixation and the size of the marine fixed nitrogen inventory

Christopher J. Somes[1] **and Andreas Oschlies**[1]

[1]GEOMAR Helmholtz Centre for Ocean Research Kiel, Kiel, Germany

Abstract Dissolved organic nitrogen (DON) and phosphorus (DOP) represent the most abundant form of their respective nutrient pool in the surface layer of the oligotrophic oceans and play an important role in nutrient cycling and productivity. Since DOP is generally more labile than DON, it provides additional P that may stimulate growth of nitrogen-fixing diazotrophs that supply fixed nitrogen to balance denitrification in the ocean. In this study, we introduce semirecalcitrant components of DON and DOP as state variables in an existing global ocean-atmosphere-sea ice-biogeochemistry model of intermediate complexity to assess their impact on the spatial distribution of nitrogen fixation and the size of the marine fixed nitrogen inventory. Large-scale surface data sets of global DON and Atlantic Ocean DOP are used to constrain the model. Our simulations suggest that both preferential DOP remineralization and phytoplankton DOP uptake are important "non-Redfield" processes (i.e., deviate from molar N:P = 16) that need to be accounted for to explain the observed patterns of DOP. Additional non-Redfield DOP sensitivity experiments testing dissolved organic matter (DOM) production rate uncertainties that best reproduce the observed spatial patterns of DON and DOP stimulate additional nitrogen fixation that increases the size of the global marine fixed nitrogen inventory by 4.7 ± 1.7% compared to the simulation assuming Redfield DOM stoichiometry that underestimates the observed nitrogen inventory. The extra 8 Tg yr^{-1} of nitrogen fixation stimulated in the Atlantic Ocean is mainly responsible for this increase due to its large spatial separation from water column denitrification, which buffers any potential nitrogen surplus in the Pacific Ocean. Our study suggests that the marine fixed nitrogen budget is sensitive to non-Redfield DOP dynamics because access to the relatively labile DOP pool expands the ecological niche for nitrogen-fixing diazotrophs.

1. Introduction

Fixed nitrogen (fixed N) is one of the major limiting nutrients that often limits biological production in the surface ocean and subsequent export production of carbon into the ocean interior. The predominant source and sink terms of the preindustrial marine fixed-N budget are nitrogen fixation (N_2 fixation) and denitrification (including anammox), respectively [*Gruber*, 2008]. Denitrification occurs in suboxic zones ($O_2 < \sim 5$ μm) in the water column and sediments when nitrate (NO_3) replaces O_2 as the electron acceptor during respiration of organic matter and is reduced to dinitrogen gas (N_2) [*Codispoti et al.*, 2001], which is not available for uptake by ordinary phytoplankton. Fixed N is supplied to the ocean by N_2-fixing diazotrophs, specialized phytoplankton that utilizes N_2 for growth [*Karl et al.*, 2002].

Spatial patterns and rates of N_2 fixation remain difficult to quantitatively constrain. Some previous methodologies used to historically measure N_2 fixation have been found to underestimate N_2 fixation by a factor of ~2 [*Mohr et al.*, 2010; *Großkopf et al.*, 2012]. Since N_2 fixation requires more energy than consumption of fixed N [*Großkopf and Laroche*, 2012] and contains a higher structural iron requirement [*Kustka et al.*, 2003], it is generally thought that diazotrophs' ecological niche will be the oligotrophic ocean where fixed N is sparse, but phosphorus and iron are still available [e.g., *Mills et al.*, 2004; *Monteiro et al.*, 2011; *Weber and Deutsch*, 2014]. *Luo et al.* [2012] presents a global compilation of N_2-fixation measurements that show high rates in these tropical regions with high atmospheric iron deposition (e.g., North Atlantic and western Pacific). However, the relative importance of phosphorus versus iron limitation is difficult to assess with the limited information on dissolved organic phosphorus, bioavailable iron distributions and elemental stoichiometry of various diazotroph communities.

In the oligotrophic ocean where N_2 fixation is abundant, dissolved organic matter (DOM) represents the largest pools of nitrogen and phosphorus [*Karl and Björkman*, 2002; *Berman and Bronk*, 2003; *Sohm and Capone*, 2010]. Since dissolved organic phosphorus (DOP) is generally more labile than dissolved organic nitrogen (DON) [*Vidal et al*., 1999, 2003; *Karl et al*., 2001; *Church et al*., 2002], DOP may relieve P limitation for phytoplankton. Preferential DOP remineralization by heterotrophic bacteria has been suggested to create an ecological niche for N_2-fixing diazotrophs by releasing additional P [*Wu*, 2000; *Mather et al*., 2008; *Monteiro and Follows*, 2012]. Some diazotrophs also have the capability to directly consume DOP that could further increase N_2 fixation in the ocean [*Cotner and Wetzel*, 1992; *Dyhrman et al*., 2006; *Sohm and Capone*, 2006]. These "non-Redfield" DON:DOP dynamics (i.e., deviating from canonical molar ratios N:P = 16:1 [*Redfield*, 1958]) could thus impact N_2 fixation, the marine fixed-N inventory, and productivity.

The current generation of global climate-biogeochemical models in the Coupled Model Intercomparison Project (CMIP, http://cmip-pcmdi.llnl.gov/) used in future projection scenarios by the Intergovernmental Panel on Climate Change (IPCC, http://www.ipcc.ch/) [e.g., *Aumont et al*., 2003; *Krishnamurthy et al*., 2009; *Ilyina et al*., 2013] typically include one semirecalcitrant pool of DOC, DON, and DOP that are produced and remineralized with constant stoichiometry near the canonical Redfield ratio. In the real ocean, DOP is more labile than DOC and DON, resulting in stoichiometries above the canonical Redfield ratio [e.g., *Clark et al*., 1998; *Church et al*., 2002; *Vidal et al*., 2003]. Therefore, these previous simple Redfield DOM schemes often produce DOP concentrations that are above observed concentrations. Since it is not standard practice to validate DOM cycling in global climate-biogeochemical models, the impacts from this stoichiometric model bias in projections of future climate scenarios are often overlooked. This may lead to deficiencies in surface nutrient cycling, and N_2 fixation, and marine productivity.

Global ocean-biogeochemical models that have accounted for non-Redfield DOP dynamics generally show enhanced N_2 fixation in the oligotrophic ocean gyres, but estimating the amount of extra N_2 fixation remains uncertain. For example, *Deutsch et al.* [2007] estimate only an ~5% increase in global N_2 fixation due to DOP* dynamics and still suggest a tight coupling between N_2 fixation and denitrification in the Pacific, although relying on DON and DOP observations mainly in the eastern subtropical North Pacific [*Abell et al*., 2000]. Whereas *Monteiro and Follows* [2012] suggest preferential DOP remineralization may result in up to a factor of 3 increase to N_2 fixation in the North Atlantic. More recently, a data assimilation study analyzing a new global compilation of DOM stoichiometry suggests that diazotroph DOP uptake may stimulate an additional $>$~20% global N_2 fixation, occurring primarily in the North Atlantic and western Pacific [*Letscher et al*., 2015].

The global model of *Landolfi et al.* [2013], which includes a dynamic N_2-fixation-denitrification feedback, suggests that a large spatial separation of N_2 fixation and denitrification is required to maintain observed marine fixed-N inventory. Since denitrification consumes ~7 mol inorganic N for each mole of respired organic N [*Richards*, 1965; *Paulmier et al*., 2009], newly fixed organic N that respires via denitrification will cause net loss to the fixed-N inventory. According to their model simulations, DOP uptake by diazotrophs in the tropical/subtropical gyres is an important factor to stimulate N_2 fixation far away from denitrification zones to balance the marine fixed-N inventory.

In this this study, we implement a slightly more complex DOM scheme than most previous studies by including DON and DOP as separate state variables to quantify the importance of non-Redfield DOM cycling in our global ocean-biogeochemical model. Large-scale data sets of DON and DOP are used to constrain sensitivity experiments that test the impact of preferential DOP remineralization and phytoplankton (including diazotrophs) DOP uptake on surface nutrient cycling, the spatial distribution of N_2 fixation, and the size of the marine fixed-N inventory.

2. Model Description

The model used here is a global coupled ocean-atmosphere-sea ice-biogeochemical model of intermediate complexity based on the University of Victoria Earth System Climate Model [*Weaver et al*., 2001] using the physical configuration and improvements to the marine ecosystem component outlined in *Keller et al.* [2012]. Additionally, we include an equatorial isopycnal mixing scheme [*Getzlaff and Dietze*, 2013] and a benthic denitrification model [*Bohlen et al*., 2012]. Each model simulation is forced for over 6000 years with

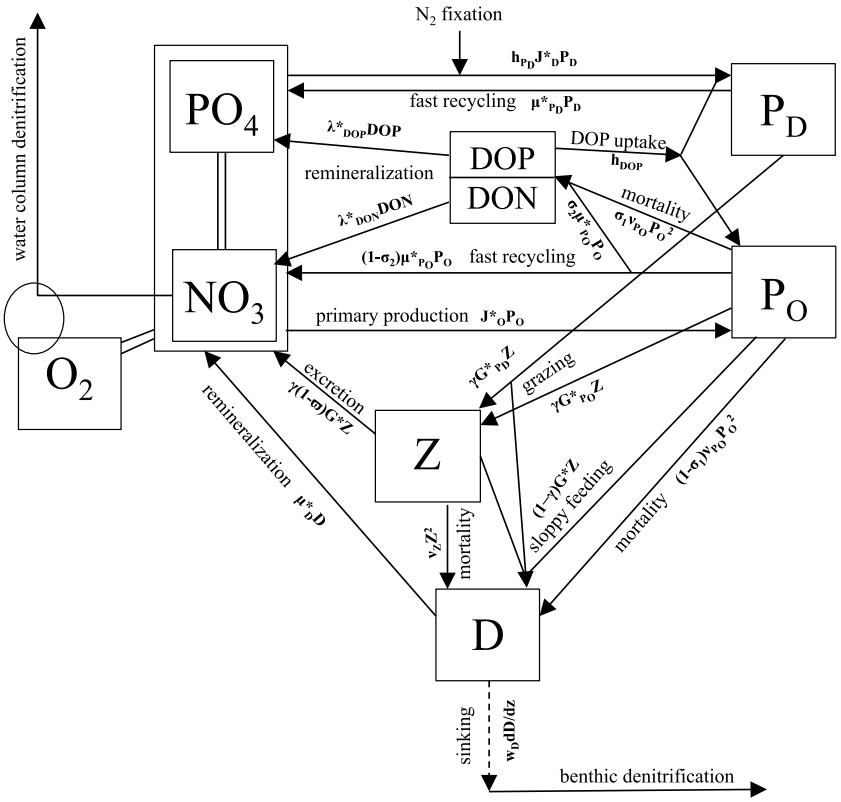

Figure 1. Schematic of the different compartments of the marine ecosystem-biogeochemical model and their interactions. See text section 2.2 for further description.

constant preindustrial boundary conditions (insolation, atmospheric CO_2, ice sheets, and monthly climatological winds [see *Eby et al.*, 2009]) until a seasonally cycling steady state is achieved. A technical description of the model is located in Appendix A, and a brief overview is provided below.

2.1. Physical Model

The physical ocean-atmosphere-sea ice model includes a three-dimensional (1.8 × 3.6°, 19 vertical levels) general circulation model of the ocean (Modular Ocean Model 2) with parameterizations such as diffusive mixing along and across isopycnals, eddy-induced tracer advection [*Gent and McWilliams*, 1990], computation of tidally induced diapycnal mixing over rough topography [*Simmons et al.*, 2004], and an anisotropic viscosity scheme [*Large et al.*, 2001] to better resolve zonal equatorial currents. This new model version also includes an anisotropic equatorial isopycnal mixing scheme to account for deep zonal equatorial jets that are not resolved by the model [*Getzlaff and Dietze*, 2013]. A two-dimensional, single-level energy-moisture balance atmosphere and a dynamic-thermodynamic sea ice model are used, forced with prescribed monthly climatological winds [*Kalnay et al.*, 1996] and ice sheets [*Peltier*, 2004].

2.2. Marine Ecosystem-Biogeochemical Model

The marine ecosystem-biogeochemical component is based on *Keller et al.* [2012]. The state variables include two phytoplankton classes, N_2-fixing diazotrophs (P_D) and ordinary phytoplankton (P_O), zooplankton (Z), particulate detritus (D), nitrate (NO_3), phosphate (PO_4), dissolved oxygen (O_2), dissolved organic nitrogen (DON), and dissolved organic phosphorus (DOP) (Figure 1). Additional tracers include dissolved inorganic carbon (DIC) and ^{14}C to constrain the carbon cycle and large-scale circulation (Figure A1). The model is run under a constant preindustrial atmospheric CO_2 concentration so there is no feedback between ocean carbonate chemistry on atmospheric CO_2 and climate in this study. Since DIC is not considered as a limiting nutrient in our model, its distribution will not affect phytoplankton growth in our preindustrial steady state simulations so we pragmatically assume a fixed C:N ratio of 6.625 for both particulate and dissolved organic

matter consistent with previous model versions. Given that oceanic DOC:DON ratios are typically higher, the modeled DOC concentrations will generally be underestimates. However, this does not have impacts on any other model variables in our simulations that are forced with fixed preindustrial atmospheric CO_2. Iron limitation of both phytoplankton classes is calculated as in *Keller et al.* [2012] using prescribed monthly mean dissolved iron concentrations estimated from the BLING model [*Galbraith et al.*, 2010] (Figure A2).

2.2.1. N_2 Fixation

Diazotrophs grow according to the same principles as the ordinary phytoplankton class in the model, but we account for their different characteristics as follows. N_2 fixation is energetically more costly than assimilating NO_3 because the strong triple-N bond must be broken down and extra respiration is required to keep the N_2-fixing compartment anoxic since O_2 inhibits the expression of the N_2-fixing nifH gene [*Großkopf and Laroche*, 2012]. Therefore, the growth rate of diazotrophs is reduced compared to ordinary phytoplankton by a handicap factor ($h_{P_D} = 0.08$; Table A1) to achieve measured growth rates consistent with culture experiments [*Breitbarth et al.*, 2007]. While the previous model version [*Keller et al.*, 2012] set diazotroph growth rates to zero below 15°C, we now allow them to grow at low rates in colder waters, following culture experiments [*Pandey et al.*, 2004; *Le Quéré et al.*, 2005].

Diazotrophs have no N limitation but are limited by P and Fe in the model. Thus, they can outcompete ordinary phytoplankton in surface waters that are depleted in NO_3 but still contain sufficient P and Fe (i.e., water with low NO_3:PO_4 from denitrification and high iron from atmospheric deposition). They will consume NO_3 when it is not limiting growth in the model, consistent with culture experiments [*Mulholland et al.*, 2001; *Holl and Montoya*, 2005]. Zooplankton grazing preference of diazotrophs is also reduced relative to the ordinary phytoplankton class to account for lower grazing on diazotrophs versus other phytoplankton (Table A1) [*O'Neil*, 1999]. Since diazotrophs are observed to have higher N:P ratios than the Redfield ratio [*Letelier and Karl*, 1998; *Sanudo-Wilhelmy et al.*, 2001], diazotroph N:P is increased to 28:1, and the excess N upon grazing and mortality of diazotrophs is routed to NO_3, while the zooplankton and detritus N:P remain at 16:1 (Table A1). Given the large range of uncertainty in some parameters, we conducted parameter sensitivity experiments (e.g., mortality rate, Fe uptake half saturation and grazing preference) and chose values that best reproduce patterns of N_2-fixation measurements [*Luo et al.*, 2012] and biogeochemical indicators of N_2 fixation (e.g., $N^* = NO_3 - 16PO_4$, $\delta^{15}N$ [see *Somes et al.*, 2010a, 2013]).

2.2.2. Denitrification

Water column denitrification (wc-denitrification) occurs when organic matter is respired in suboxic zones. We use a threshold of 3 μm O_2 that sets where respiration of organic matter occurs equally between wc-denitrification and aerobic respiration. Further below (above) this threshold, a greater fraction of wc-denitrification (aerobic respiration) occurs. Note that complete aerobic respiration occurs above 7 μm O_2 (equation (A11)). The threshold value of 3 μm O_2 is slightly lower than previous model versions that used 5 μm O_2 because historical measurement techniques overestimated O_2 concentrations in suboxic zones [*Codispoti and Christensen*, 1985; *Bianchi et al.*, 2012]. This lower threshold decreases the simulated global wc-denitrification rate by ~20%. NO_3 never becomes fully depleted in suboxic zones in this model version due in part to this lower O_2 threshold, but mainly as a result of improved equatorial circulation dynamics from the anisotropic zonal isopycnal mixing parameterization [*Getzlaff and Dietze*, 2013], which results in simulated global volume of the suboxic zones within the observational uncertainty (Table 3). Therefore, we are able to use a lower wc-denitrification reduction NO_3 threshold of 3 μm compared to *Somes et al.* [2013] that used values a high as 32 μm. Note that NO_3 is never consumed to 3 μm in suboxic zones of the model simulations presented here and thus the NO_3 threshold has no impact on the wc-denitrification rates in this study.

Anammox is also removing dissolved inorganic N in these areas of low-oxygen and high-organic matter recycling [*Thamdrup and Dalsgaard*, 2002]. Although the exact partitioning between wc-denitrification and anammox is not well known, anammox likely depends on nitrate reduction ($NO_3 \rightarrow NO_2$), the first step of wc-denitrification, to supply sufficient nitrite that typically exists in low concentrations [*Lam et al.*, 2009]. It has been found that the ultimate driver for N loss in suboxic zones is organic matter respiration [*Kalvelage et al.*, 2013] and whether the N-loss process occurs as anammox or denitrification has little consequence on the net biogeochemical system [*Koeve and Kähler*, 2010]. Since our model does not differentiate between different species of dissolved inorganic nitrogen, this wc-denitrification parameterization is designed to capture total fixed-N loss from wc-denitrification and anammox.

Table 1. DOM Model Experiment Parameters[a]

Experiment Number	Experiment Name	$\sigma 1_{DOM}$	$\sigma 2_{DOM}$	$\lambda 0_{DOP}$ (yr^{-1})	$\lambda 0_{DON}$ (yr^{-1})	h_{DOP}
1	RedDOM	0.1	0	0.00342	0.00342	0
2	pref_DOP_remin	0.1	0	0.00684	0.00342	0
3	nonRedDOP	0.1	0	0.00684	0.00342	0.4
4	low_nonRedDOP	0.075	0	0.00684	0.00342	0.4
5	high_nonRedDOP	0.125	0	0.00684	0.00342	0.4
6	fast_nonRedDOP	0.1	0.16	0.0684	0.0342	0.4

[a]Fraction of phytoplankton mortality routed to DOM ($\sigma 1_{DOM}$), fraction of microbial fast-recycling routed to DOM ($\sigma 2_{DOM}$), SR-DOM remineralization rate at 0°C ($\lambda 0$), and DOP uptake growth rate handicap factor (h_{DOP}).

Benthic denitrification (ben-denitrification) is included using a empirical function deduced from benthic flux measurements [*Bohlen et al.*, 2012]. This function estimates benthic denitrification from organic carbon rain rate into the sediments and bottom water O_2 and NO_3 concentrations (equation (A12)). It provides an efficient alternative to coupling a full sediment model that would significantly increase computational costs. Note that all organic matter instantaneously remineralizes in the bottom water when it reaches the seafloor. NO_3 is then removed from the bottom water according to this ben-denitrification function. We also include a subgrid-scale bathymetry mask within this ben-denitrification scheme to account for shallow continental shelves and other topographical features that are not fully resolved in the model's coarse-resolution grid [see *Somes et al.*, 2010b].

2.3. Dissolved Organic Matter Model Configuration

We implement semirecalcitrant dissolved organic matter pools of phosphorus (SR-DOP) and nitrogen (SR-DON) into the model. This SR-DOM scheme adds two new state variables to the model, DOP and DON (Figure 1), and indirectly accounts for DOC by assuming it is produced and remineralized at the C:N ratio of 6.625 relative to DON. While bulk DOM is commonly observed to contain higher C:N ratios [e.g., *Church et al.*, 2002; *Sannigrahi et al.*, 2005], the semirecalcitrant DOC:DON pool is estimated to be 7.5 in the euphotic zone [*Letscher et al.*, 2015]. Here we force the model with constant preindustrial atmospheric CO_2 that makes climate-carbon-biogeochemical feedback inactive. Since DIC is not a limiting nutrient in the model, its distribution will not affect biological production in the preindustrial steady state simulations so we pragmatically chose a DOC:DON ratio consistent with the other organic matter variables, but note that a more realistic ratio should be used in climate change simulations.

SR-DOM is produced from a constant fraction ($\sigma 1_{DOM}$) of the ordinary phytoplankton mortality rate and the microbial fast-recycling loop ($\sigma 2_{DOM}$) in the model (Table 1), with the elemental stoichiometry of phytoplankton (molar $R_{N:P} = 16$; Table A1). We assume that other processes that contribute to the labile DOM pool (e.g., excretion) are recycled on shorter time scales. Since this labile DON and DOP pools can be consumed by phytoplankton [*Dyhrman et al.*, 2006; *Bronk et al.*, 2007], we route this labile DOM directly into inorganic nutrients to save computation costs of explicitly including additional DOM state variables following *Schmittner et al.* [2005].

Recalcitrant DON and DOP that remain in the deep ocean longer than the time scale of the large-scale ocean circulation (>~1000 years) are not accounted for in the model because of its uncertain removal mechanisms and its low concentrations in the deep Pacific where this pool accounts for the majority of the total DOM. For example, *Clark et al.* [1998] report DON and DOP concentrations of 0.45 μm and 0.015 μm, respectively, at 4000 m in the tropical South Pacific. *Letscher et al.* [2015] compile a global DOM database and report average recalcitrant DON and DOP concentrations of 1.8 μm and 0.03 μm, respectively. They estimate that only ~1% of total DOM produced is recalcitrant, and it remineralizes according to Redfield stoichiometry in the surface ocean due to photooxidation, which suggest that it will not play a significant role in non-Redfield nutrient cycling in the surface ocean. Since it is currently unclear which fraction of different recycling processes contribute to the labile, semirecalcitrant, recalcitrant, and ultrarecalcitrant DOM pools [see *Hansell*, 2013], we chose to implement a relatively simple SR-DOM scheme and test different production and remineralization rates of the SR-DOP and SR-DON pools.

Large variability of DOM observations throughout the oceans makes setting the initial DOP and DON conditions uncertain. Observations of DOP range from 0.1 to 0.4 and 0.015 to 0.15 μm in the surface ocean and deep

ocean, respectively [*Clark et al.*, 1998; *Benner*, 2002]. We account only for SR-DOM in the model so the model was initialized using low-end DOP values of 0.1, 0.025, and 0.005 μm in the surface (0–130 m), intermediate (130–1000 m), and deep ocean (1000–6000 m), respectively. While total phosphorus is conserved in the model, the model's dynamic fixed-N cycle with N_2 fixation and denitrification will reach its own equilibrium state based on the parameters and phosphorus inventory. The SR-DON pool is initialized with values of 4.8, 1.2, and 0.24 μm in the surface, intermediate, and deep ocean, respectively. Provided that for a given phosphorus inventory and set of model parameters and equations only a single steady state solution exists, for which we could not find any contradictory evidence, the initial SR-DON conditions only determine how long it takes for the model to reach steady state but does not affect the steady state solution.

2.3.1. Redfield DOM

In the baseline experiment #1 (RedDOM), both production and remineralization of DOM occur at the Redfield N:P = 16 ratio. Remineralization rate (λ) of DOM is temperature (T) dependent, $\lambda = \lambda 0 \times \exp(T/T_b)$, with the same e-folding temperature as in the remineralization rate for sinking detrital matter ($T_b = 15.56$°C). We chose a remineralization rate following *Letscher et al.* [2013], who compiled available DON observations and suggest that the majority of the surface DON is recalcitrant and must subduct before it can be remineralized to inorganic nitrogen. In our coupled ocean circulation-biogeochemical model that applies a temperature-dependent DOM remineralization at all locations, this is achieved with a rate $\lambda 0 = 0.00684\ \mathrm{yr}^{-1}$ at 0°C (146 year lifetime) (Table 1) that increases to $\lambda = 0.045\ \mathrm{yr}^{-1}$ (22 year lifetime) at 30°C. This is longer than the 15 year surface semilabile DON lifetime estimated by *Letscher et al.* [2015], which suggests that our simulated SR-DON contains a slightly more refractory component of total DON compared to that study. This temperature-dependent SR-DOM remineralization rate allows most of the surface SR-DON to subduct below the euphotic zone but completely remineralizes before it reaches the deep North Pacific that is composed mainly of recalcitrant DOM (Figure 2). The DOM production factor was chosen to produce DON concentrations that remain lower than total observed concentration (Figure 3) because our model only simulates the semirecalcitrant fraction of the total DOM pool.

2.3.2. Non-Redfield DOP

Experiment #2 (pref_DOP_remin) was designed to test the importance of preferential DOP remineralization [*Vidal et al.*, 1999, 2003; *Wu*, 2000] on N_2 fixation by increasing the remineralization rate of SR-DOP ($\lambda 0_{DOP}$) by a factor of 2 relative to SR-DON (Table 1). Experiment #3 (nonRedDOP) introduces the ability for both ordinary phytoplankton and diazotrophs to consume DOP, consistent with observations [*Cotner and Wetzel*, 1992; *Dyhrman et al.*, 2006; *Martiny et al.*, 2006; *Sohm and Capone*, 2006], together with preferential DOP remineralization (Table 1). Since converting DOP to biomass requires more energy than PO_4 [*Moore et al.*, 2005], we apply an additional handicap for DOP uptake by lowering their growth rates by a factor of 0.4 in the simulation nonRedDOP (Table 1). Both phytoplankton classes will consume the form of P that allows them to grow most efficiently (equations (A1) and (A2)). The effect of phytoplankton DOP uptake alone can be evaluated by comparing experiment #3 (nonRedDOP) with experiment #2 (pref_DOP_remin).

2.3.3. Non-Redfield DOP Production/Remineralization Sensitivity

Additional non-Redfield DOP experiments (#4–6) were designed to test the sensitivity to DOM production and remineralization rates (Table 1). Experiments #4 and #5 change the DOM production factor by −25% (low_nonRedDOP) and +25% (high_nonRedDOP), respectively. In our final fast-recycling experiment #6, the remineralization rate of DOM is increased by an order of magnitude to test the impacts of simulating a more labile pool of DOM (fast_nonRedDOP). Since this DOM remineralizes much faster, we include higher production rates by directing organic matter from the fast-recycling microbial loop parameterization to achieve similar surface concentrations in the tropical ocean as in experiment #3 nonRedDOP (Table 2).

3. Results and Discussion

3.1. DOM Evaluation

3.1.1. Observational Data Sets

Because we include non-Redfield DOM dynamics, we evaluate DOP and DON with separate data sets. We use a database of DON that covers the global surface ocean [*Letscher et al.*, 2013] to constrain DON cycling in the model. The data were collected on numerous cruises throughout all seasons as part of the U.S. Global Ocean Carbon and Repeat Hydrography program (http://ushydro.ucsd.edu/). However, few locations contain data

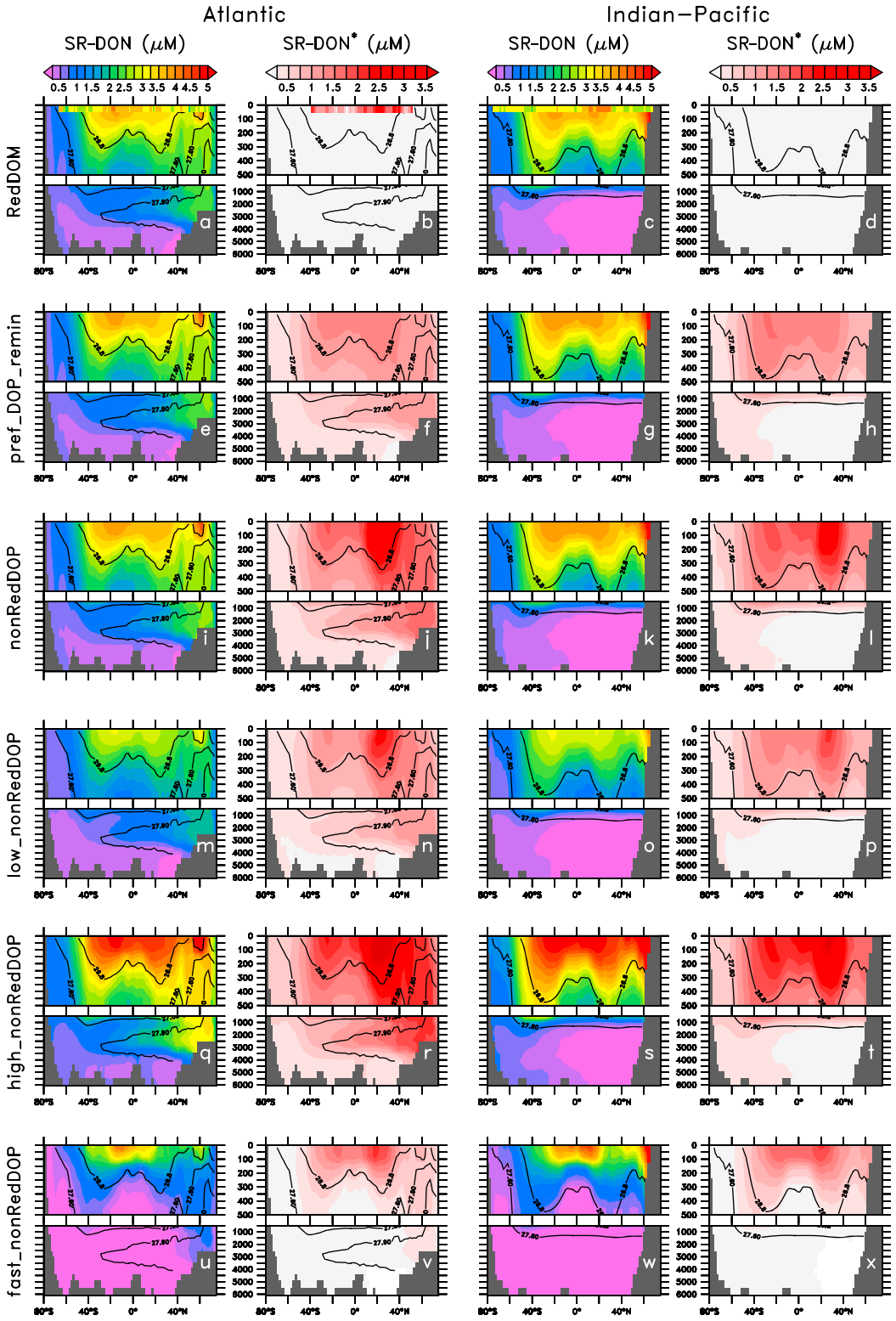

Figure 2. Annual zonally averaged semirecalcitrant (SR) DON and SR-DON* = SR-DON – 16SR-DOP from (a–d) Redfield DOM (RedDOM), (e–h) preferential DOP recycling (pref_DOP_remin), (i–l) preferential DOP recycling and phytoplankton DOP uptake (nonRedDOP), (m–p) non-Redfield DOP with low DOM production (low_nonRedDOP), (q–t) non-Redfield DOP with high DOM production (high_nonRedDOP), and (u–x) fast recycling non-Redfield DOP (fast_nonRedDOP) with available surface observations (0–50 m; Figures 2a–2c) by removing the assumed recalcitrant pool of DON (1.25 μm) and DOP (25 nm) from total observations, which are median values from the observational uncertainty range (see section 3.1.1). Sigma-theta potential density contour lines of 26.8, 27.6, and 27.9 kg m^{-3} are shown as a function of latitude and depth.

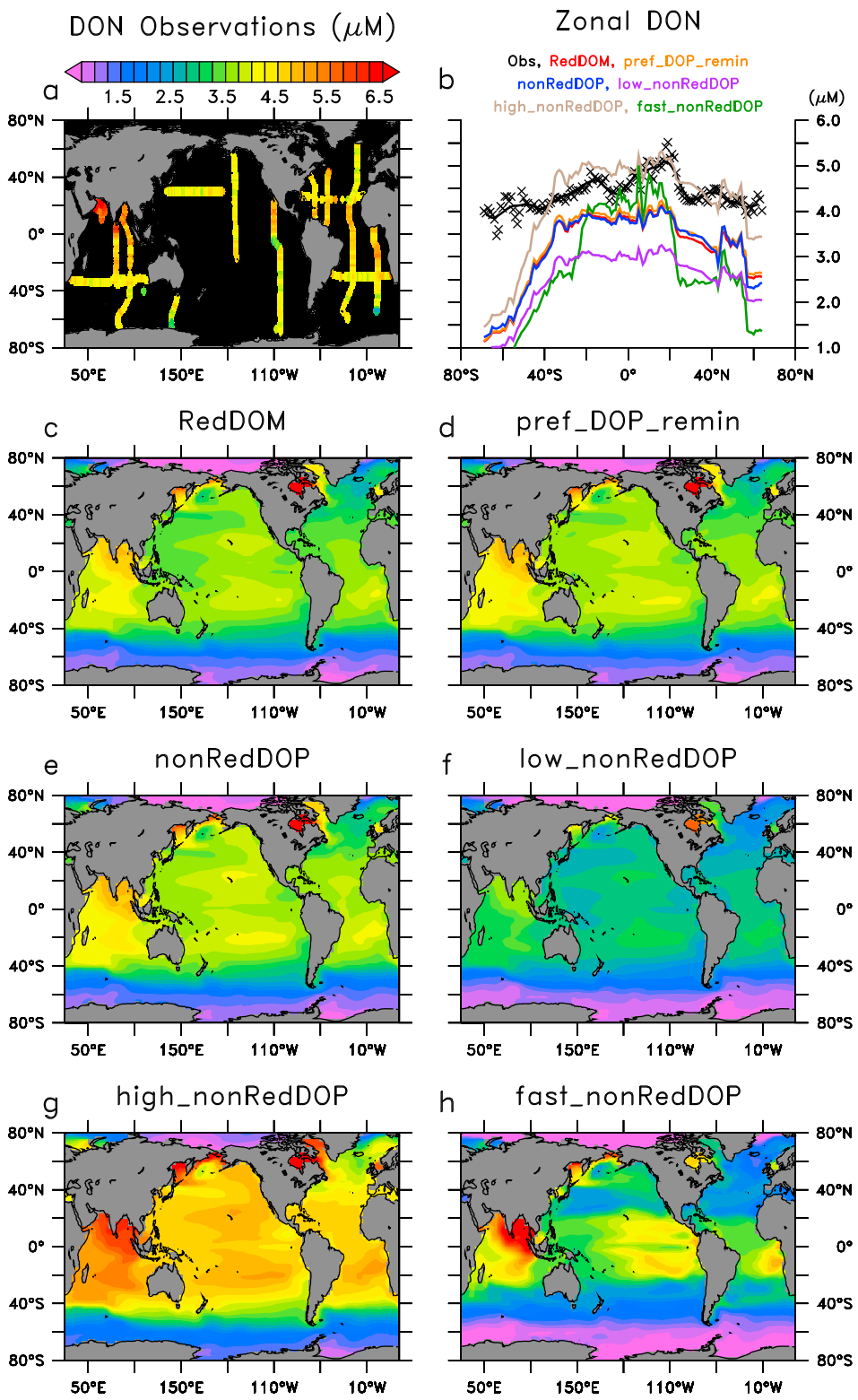

Figure 3. Comparison of surface (0–50 m) (a) map and (b) zonally averaged DON observations [*Letscher et al.*, 2013] with annual semirecalcitrant DON from the model experiments (c) Redfield DOM (RedDOM), (d) preferential DOP remineralization (pref_DOP_remin), (e) preferential DOP recycling and phytoplankton DOP uptake (nonRedDOP), (f) non-Redfield DOP with low DOM production (low_nonRedDOP), (g) non-Redfield DOP with high DOM production (high_nonRedDOP), and (h) fast recycling non-Redfield DOP (fast_nonRedDOP). Note that the zonally averaged model results in Figure 3b are taken only from locations where observations exist.

Table 2. Global Dissolved Organic Matter Results[a]

Experiment Number	Experiment Name	PO_4 (μm)	Global SR DOP (nm)	Data-Masked North Atlantic Surface DOP (nm)	Data-Masked South Atlantic Surface DOP (nm)	Global SR DON (μm)	Data-Masked Tropical Surface DON (μm)	Data-Masked Extratropical Surface DON (μm)
-	Observational Estimate	2.17[b]	~15–50[c]	90.4[d]	156[d]	~0.5–2.5[e]	4.79[f]	4.29[f]
1	RedDOM	2.14	52.0	204	219	0.829	3.90	3.27
2	pref_DOP_remin	2.16	23.9	129	148	0.850	3.99	3.37
3	nonRedDOP	2.17	19.6	55.8	130	0.867	4.04	3.45
4	low_nonRedDOP	2.17	15.0	45.9	101	0.649	3.05	2.60
5	high_nonRedDOP	2.16	24.2	64.9	158	1.08	5.01	4.30
6	fast_nonRedDOP	2.18	5.96	58.7	106	0.211	4.27	2.37

[a]Annual model average after 6000 years of simulation time. "Data-masked" model results only include locations where observations exist.
[b]From World Ocean Atlas 2009 [*Garcia et al.*, 2010a].
[c]Range of values at intermediate depth reported in *Karl and Björkman* [2002].
[d]From *Mather et al.* [2008].
[e]Range of values at intermediate depth reported in *Berman and Bronk* [2003].
[f]From *Letscher et al.* [2013].

from all seasons. In the subtropical North Pacific, *Church et al.* [2002] show negligible seasonal cycles of DOC, DON, and DOP over an entire decade (1989–1999), which suggests that there is not a significant seasonal cycle of DOM in tropical/subtropical open ocean locations where N_2 fixation is most abundant, which is the focus of this study. Interannual variability accounted for the main variability in DOM, which may be the largest source of uncertainty with the model-data comparison. There is a sampling bias with most cruises in the high-latitude Southern Ocean transects taking place in austral summer. The observed patterns of DON show higher values in the tropical/subtropical open ocean with a notable maximum in the North Indian Ocean and moderate to low values toward the middle to high latitudes (Table 2 and Figure 3a).

To validate the DOP patterns in the model, we use a data set from the Atlantic Ocean [*Mather et al.*, 2008] that consists of five cruises during spring (April–June) and two cruises during autumn (October–November) as part of the Atlantic Meridional Consortium Program (http://www.bodc.ac.uk/projects/uk/amt/). We show the annual average here (i.e., each month of data has equal weight) but acknowledge that this is not true annual average and some seasonal bias may exist. Since the DOP data were collected in opposite seasons, it may not be far from the true annual average. The main pattern shows highest DOP in the Southern Tropical Atlantic with an interhemispheric asymmetry of lower DOP concentrations in the tropical/subtropical North Atlantic (Table 2 and Figure 4a).

Since the DOM model configuration includes only the semirecalcitrant fraction of the DOM pool, the observations provide an upper limit on the simulated SR-DOM concentrations. Uncertainties of the magnitude of the different recalcitrant DOM pools make it difficult to determine how much lower the model SR-DOM concentrations should be relative to the total DOM observations. Assuming that all DON in the deep Pacific Ocean (~0.5–2.0 μm [*Clark et al.*, 1998; *Karl et al.*, 2001; *Letscher et al.*, 2015]) is recalcitrant, which is not included in the model, the simulated SR-DON should then be lower than observations of total DON by about this range. DOP observations in the deep Pacific Ocean are typically in the range of ~15–40 nm [*Clark et al.*, 1998; *Karl et al.*, 2001; *Karl and Björkman*, 2002], which represents a large source of uncertainty in the model-data comparison.

3.1.2. Redfield DOM

The RedDOM simulation produces SR-DON:DOP stoichiometry according to the Redfield ratio, which yields SR-DON* = SR-DON − 16SR-DOP values of 0, which underestimate observations in the Atlantic (Figures 2b and 2d). While the spatial trends of DON observations are generally reproduced (Figure 3), discrepancies of simulating DOP are apparent (Figure 4). For example, RedDOM overestimates the magnitude of DOP concentrations throughout the entire Atlantic. According to these observational data sets, DOP exists at concentrations lower than the canonical Redfield ratio relative to DON so this model bias likely occurs in all DOM models that assume constant elemental Redfield stoichiometry of DOP relative to DOC or DON.

3.1.3. Non-Redfield DOP

More efficient DOP remineralization in experiment pref_DOP_remin reduces surface SR-DOP concentrations (Figure 4d), which become more consistent with observations. This results in higher SR-DON:DOP stoichiometries throughout all tropical/subtropical ocean basins (Figures 2f and 2h). However, model

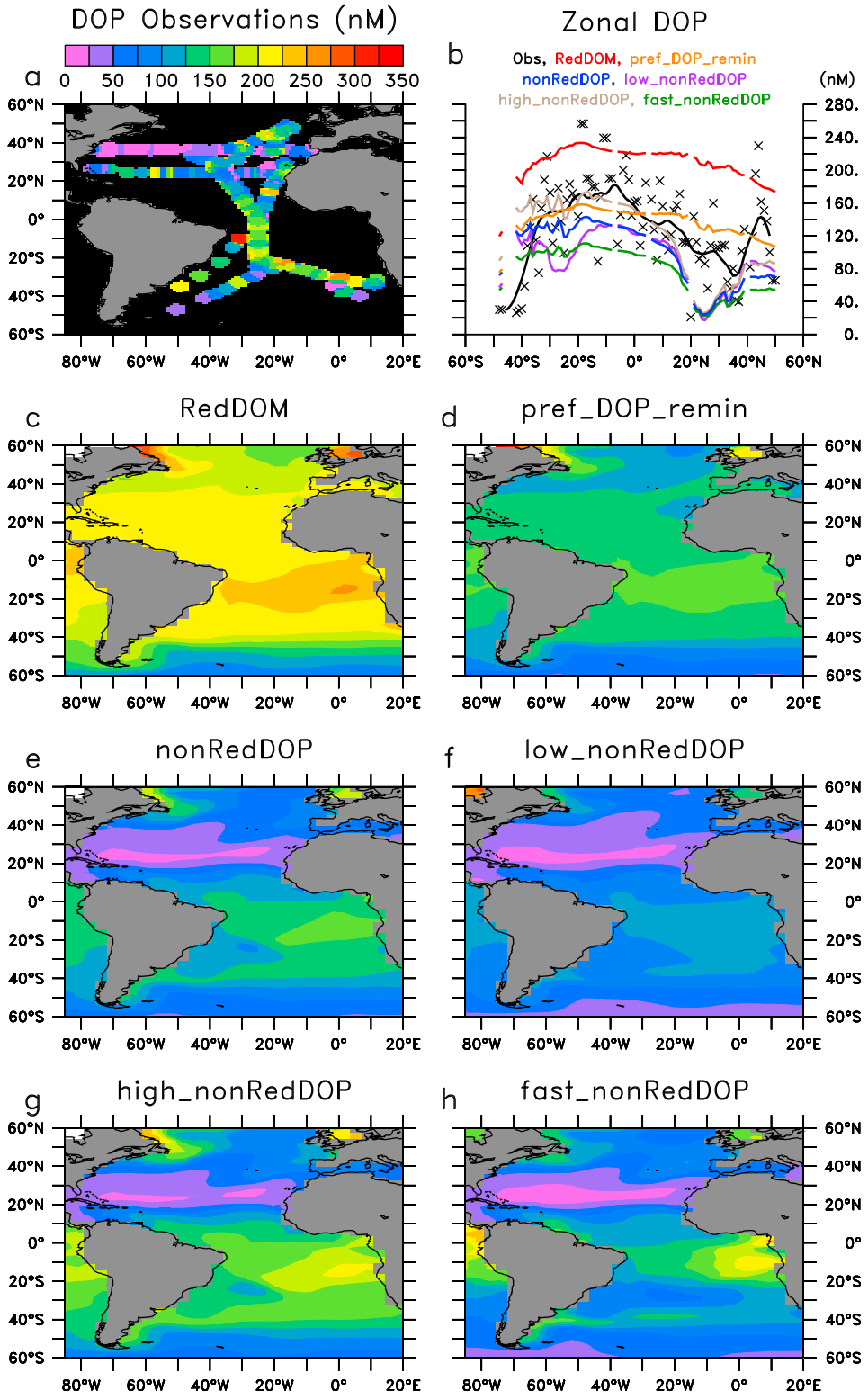

Figure 4. Comparison of surface (0–50 m) (a) map and (b) zonally averaged DOP observations [*Mather et al.*, 2008] with annual semirecalcitrant DOP from the model experiments (c) Redfield DOM (RedDOM), (d) preferential DOP remineralization (pref_DOP_remin), (e) preferential DOP remineralization and phytoplankton DOP uptake (nonRedDOP), (f) non-Redfield DOP with low DOM production (low_nonRedDOP), (g) non-Redfield DOP with high DOM production (high_nonRedDOP), and (h) fast recycling non-Redfield DOP (fast_nonRedDOP). Note that the zonally averaged model results in Figure 4b are taken only from locations where observations exist.

experiment pref_DOP_remin alone fails to reproduce the full extent of the observed meridional asymmetry of SR-DOP and SR-DON* across the Atlantic suggesting that additional non-Redfield DOM cycling processes are needed.

Only the model experiments including phytoplankton DOP uptake (nonRedDOP) reproduce the full extent of observed asymmetry of lower DOP (Figures 4e–4g), as well as higher SR-DON:DOP stoichiometries (Figures 2i–2t), in the North versus South Atlantic. Phytoplankton are able to consume more DOP in the North Atlantic because Fe limitation is lower due to atmospheric Fe deposition originating from the Saharan desert [*Mahowald et al*., 2009], whereas the South Atlantic is more Fe limited [*Moore et al*., 2009] (Figure A2). This non-Redfield DOP configuration is generally consistent with *Mather et al.* [2008], who suggest higher utilization of DOP by diazotrophs in the North Atlantic. Our model simulations suggest that preferential DOP remineralization and phytoplankton DOP uptake are both important processes that control the observed surface DOP distribution in the Atlantic. This is in contrast to *Letscher et al.* [2015], who estimate that SR-DOP has a longer lifetime than SR-DON in the euphotic zone in the absence of phytoplankton DOP uptake that accounts for reduced DOP concentrations in their model.

3.1.4. Non-Redfield DOP Production Sensitivity

The DOM production factor determines how much DOM is produced and circulates around the surface ocean. The low_nonRedDOP (high_nonRedDOP) simulation produces less (more) SR-DOP that can be consumed by ordinary phytoplankton and diazotrophs, resulting in lower (higher) SR-DON:DOP stoichiometries (Figure 2). Low_nonRedDOP produces SR-DON concentrations that are lower than total DON observations by ~2 μm (Table 2 and Figures 3b and 3f). It would be the most consistent with DON observations assuming a high-end fraction for recalcitrant DOM, which determines how much lower the simulated SR-DON concentrations should be relative to total DON observations. On the other hand, high_nonRedDOP predicts surface SR-DON concentrations near the total observed magnitude throughout the tropical/subtropical ocean (Table 2 and Figures 3b and 3g), which can be considered an upper estimate for SR-DON.

3.1.5. Fast Recycling Non-Redfield DOP

The fast recycling DOM experiment (fast_nonRedDOP) uses remineralization rates of DON and DOP that are generally more similar to other global climate-biogeochemical models [e.g., *Ilyina et al*., 2013; *Landolfi et al*., 2013] compared to our previous experiments. They produce higher DOM concentrations in the tropical regions due to higher production rates assumed for the more labile fast recycling DOM pool and lower concentrations in the subtropical ocean and higher latitudes due to faster remineralization rates. The lower SR-DOP concentrations in the oligotrophic ocean gyres (Figure 4h) reduce SR-DOP uptake by phytoplankton, resulting in lower SR-DON:DOP stoichiometries as well (Figures 2v and 2x). The large gradient of DON in the fast_nonRedDOP between the tropics and extratropics is in contrast to the observations, which show elevated concentrations throughout the subtropical ocean (Table 2 and Figure 3b). This suggests that including only a faster recycling semilabile DON pool is insufficient to reproduce observed surface DON patterns and highlights the importance of using large-scale data sets to constrain the model parameters and simulated trends.

3.2. Influence on the Distribution of N_2 Fixation and the Marine Fixed-N Inventory

3.2.1. Redfield DOM

The RedDOM simulation predicts a reduced size of the marine fixed-N inventory by 3.4% relative to initial conditions set by World Ocean Atlas Observations (Table 3 and Figure 5) because N_2 fixation is initially too low to balance denitrification. It does not predict N_2 fixation to the full extent north of 10° in the tropical North Atlantic according to N_2-fixation rate measurements [*Luo et al*., 2012] (Figure 6c). The reduced size of the marine fixed-N inventory in RedDOM is caused by the persisting deficit of the fixed-N budget in the Atlantic Ocean (Figure 5b). Here much of the fixed-N deficiency from denitrification, some of which occurring in high-latitude sediments, is not immediately balanced by N_2 fixation and subducts with North Atlantic deepwater formation. These fixed-N deficient waters eventually circulate into the Pacific and Indian Oceans, stimulating additional N_2 fixation to generate a surplus in those basins (Figures 5c and 5d).

3.2.2. Non-Redfield DOP

Preferential DOP remineralization and DOP uptake by phytoplankton relieves P limitation that benefits diazotrophs in N-limiting conditions. When including only preferential DOP remineralization (pref_DOP_remin), the ecological niche for diazotrophs expands in all ocean basins, which stimulates an additional

Table 3. Global Fixed Nitrogen Inventory Results[a]

Experiment Number	Experiment Name	NO_3 (μm)	NPP (Gt C yr^{-1})	Suboxic Volume ($\times 10^{14}$ m^3)	N_2 Fixation (Tg N yr^{-1})	WC Denitrification (Tg N yr^{-1})	Benthic Denitrification (Tg N yr^{-1})
-	Observational Estimate	31.0[b]	36–57[c]	7.5–30[d]	130–225[e]	50–75[e]	90–210[e]
1	RedDOM	29.95	52.4	6.70	101	33.7	67.1
2	pref_DOP_remin	30.66	54.8	11.5	120	49.9	69.7
3	nonRedDOP	31.35	56.3	15.5	131	59.4	71.7
4	low_nonRedDOP	30.84	56.7	14.5	132	59.3	72.3
5	high_nonRedDOP	31.85	56.0	17.0	131	59.8	71.2
6	fast_nonRedDOP	31.21	55.4	10.6	118	48.0	69.9

[a]Annual model average after 6000 years of simulation time.
[b]From World Ocean Atlas 2009 [*Garcia et al.*, 2010a].
[c]From *Antoine et al.* [1996], *Falkowski et al.* [2003], and *Gregg* [2003].
[d]From World Ocean Atlas 2009 [*Garcia et al.*, 2010b; *Bianchi et al.*, 2012].
[e]Range from *Bianchi et al.* [2012], *Eugster and Gruber* [2012], *DeVries et al.* [2013], and *Somes et al.* [2013].

19 Tg N yr^{-1} of N_2 fixation that increases the size of the marine fixed-N inventory by 2.4% relative to RedDOM (Figures 5a and 6e). The nonRedDOP experiment gives phytoplankton (including diazotrophs) the ability to consume SR-DOP together with preferential DOP remineralization, which further increases N_2 fixation by an additional 11 Tg N yr^{-1} relative to pref_DOP_remin. While the ordinary phytoplankton class accounts for 87% of DOP consumption in the model, diazotrophs are responsible for the remaining DOP uptake. If diazotrophs are able to consume a larger fraction of total DOP uptake in the real ocean, our model would be underestimating its potential to stimulate extra N_2 fixation.

Since DOP uptake occurs where PO_4 is the major limiting nutrient for diazotrophs, its effect is determined by the Fe and P limitation parameters that have large uncertainties. In our model configuration, the North Atlantic and western North Pacific are the main regions where PO_4 limitation is stronger than Fe limitation (Figure A2) due to high rates of atmospheric Fe deposition from the Saharan and Gobi deserts [*Mahowald et al.*, 2009], respectively. This is where most of the additional N_2 fixation is stimulated with respect to pref_DOP_remin (Figure 6e) and may explain why previous models without phytoplankton DOP uptake [e.g., *Moore and Doney*, 2007; *Keller et al.*, 2012; RedDOM from this study] were unable to simulate N_2 fixation to the full spatial extent north of 10° in the tropical North Atlantic according to N_2-fixation measurements [*Luo et al.*, 2012].

The increase in global N_2 fixation (30%) is much higher than the size of the marine fixed-N inventory (4.7%) in nonRedDOP relative to RedDOM due to the dynamic N_2-fixation-denitrification feedback in the model. Higher N_2-fixation rates in nonRedDOP increases productivity near denitrification zones due to extra fixed N in surface waters. This additional productivity in turn, further increases denitrification and reduces the net surplus to the marine fixed-N inventory (Figures 5 and 6).

The strength of this feedback depends on the spatial separation of N_2 fixation to denitrification. If all of the newly fixed N from N_2 fixation is directly respired in the suboxic zones via wc-denitrification, there will be a net loss to the marine fixed-N inventory because denitrification consumes ~7 mol N for each mole of respired organic N [*Landolfi et al.*, 2013]. In the Pacific Ocean where the major suboxic zones exist in the model, additional productivity due to more N_2 fixation stimulates even higher wc-denitrification rates relative to N_2 fixation. Although the largest increase to N_2 fixation occurs in the Pacific, this N-cycle feedback prevents the fixed-N budget of the Pacific from becoming a net source and switches it to a net sink of fixed N in nonRedDOP (Figure 5). Our simulations suggest the importance of including a dynamic N_2-fixation-denitrification feedback [*Landolfi et al.*, 2013], which are often not accounted for in some ocean biogeochemical models (e.g., not diagnosing direct impacts of denitrification [*Dutkiewicz et al.*, 2014] or imposing fixed wc-denitrification rates from a separate inverse model [*Weber and Deutsch*, 2014]).

The additional 8 Tg N yr^{-1} N_2 fixation stimulated in the Atlantic Ocean in nonRedDOP is responsible for the increase in the size of the marine fixed-N inventory due to its large spatial separation from suboxic zones occurring primarily in the Pacific. Therefore, the stabilizing feedback of increasing wc-denitrification in response to additional N_2 fixation to balance the fixed-N budget is relatively weak in the Atlantic compared to the Pacific. This allows the additional fixed N from N_2 fixation in the Atlantic to remain in the

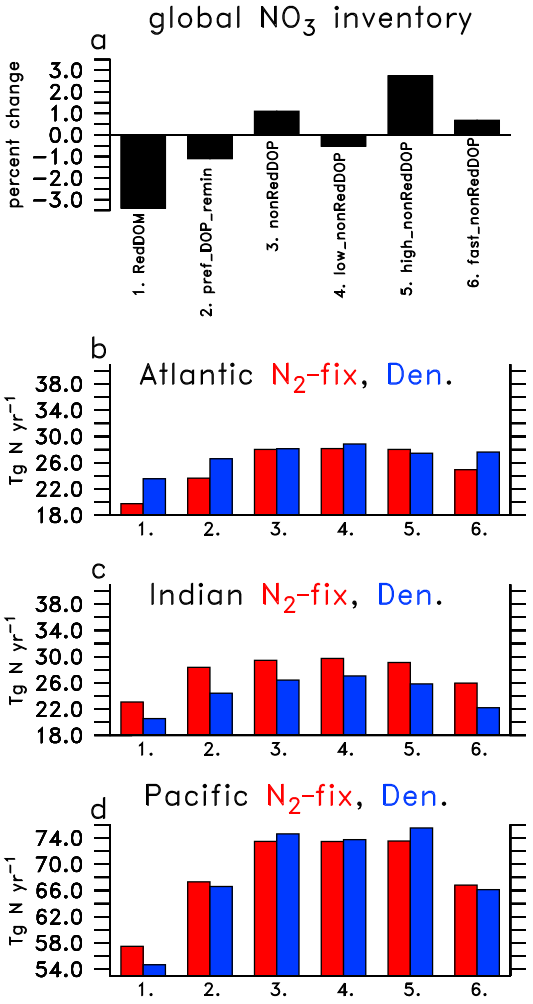

Figure 5. (a) The global NO_3 inventory change relative to initial condition estimate from the World Ocean Atlas 2009 and rate of N_2 fixation (left red bar) and total denitrification (right blue bar) in the (b) Atlantic Ocean, (c) Indian Ocean, and (d) Pacific Ocean from the model experiments: (1) Redfield DOM (RedDOM), (2) preferential DOP remineralization (pref_DOP_remin), (3) preferential DOP remineralization and phytoplankton DOP uptake (nonRedDOP), (4) non-Redfield DOP with low DOM production (low_nonRedDOP), (5) non-Redfield DOP with high DOM production (high_nonRedDOP), and (6) fast recycling non-Redfield DOP (fast_nonRedDOP). In each model experiment, ~0.2 Tg N yr^{-1} of N_2 fixation and ~1.9 Tg N yr^{-1} of benthic denitrification occur in the Arctic Ocean.

ocean for longer time scales and contribute to a surplus in the size of the marine fixed-N inventory before it eventually circulates back into suboxic zones.

3.2.3. Non-Redfield DOP Production Sensitivity

The low and high DOM production sensitivity experiments produce different spatial patterns of N_2 fixation that cause changes to the global NO_3 inventories relative to nonRedDOP. In low_nonRedDOP (high_nonRedDOP), reduced (enhanced) production of SR-DOP available for uptake by diazotrophs results less (more) N_2 fixation (Figure 6g (Figure 6i)), as well as lower (higher) SR-DON:DOP stoichiometries. Since these changes to N_2 fixation mainly occur in the North Atlantic and western North Pacific, far away from the denitrifying eastern tropical Pacific suboxic zones, they are not immediately compensated by changes in denitrification and generate a smaller (larger) marine fixed-N inventory (Figure 5a). However, some of the reduced (enhanced) N_2 fixation in parts of the North Pacific in low_nonRedDOP (high_nonRedDOP) drive less (more) productivity and resulting denitrification in the eastern Pacific suboxic zones (Figure 6h (Figure 6j)). This N_2-fixation-denitrification feedback partially buffers the potential impact of N_2-fixation changes alone on the marine fixed-N inventory.

Denitrification is also affected by changes to SR-DON production, but it has a smaller impact on the global marine fixed-N inventory compared to N_2 fixation changes caused via diazotroph SR-DOP uptake. Lower (higher) SR-DON production relieves (increases) N limitation and thereby causes slightly more (less) productivity and denitrification near the continental shelves (Figure 6h (Figure 6j)). This denitrification change is compensated by N_2 fixation and causes slightly enhanced (reduced) N_2 fixation in some locations in low_nonRedDOP (high_nonRedDOP), most notably in the western equatorial Atlantic Ocean (Figure 6g (Figure 6i)).

3.2.4. Fast Recycling Non-Redfield DOP

The fast recycling non-Redfield DOP simulation predicts less N_2 fixation compared to the regular non-Redfield DOP experiment that results in a reduction the size of the marine fixed-N inventory (Figure 5). With faster DOM remineralization rates, SR-DOP recycles more efficiently back PO_4, which reduces SR-DOP uptake by diazotrophs and results in less N_2 fixation (Figure 6k). Higher DOM production rates in fast_nonRedDOP increase SR-DON concentrations near the suboxic zones in the eastern North Pacific and Indian Oceans, which in turn increases N limitation and reduces productivity and wc-denitrification (Figures 3h and 6l). Elevated DOM concentrations transport nutrients away from the productive tropical regions that reduces "nutrient trapping" and production there [*Najjar et al.*, 1992; *Dietze and Loeptien*, 2013]. However, these experiments produce SR-DON concentrations that overestimate the observations near the suboxic zones (Figure 3h).

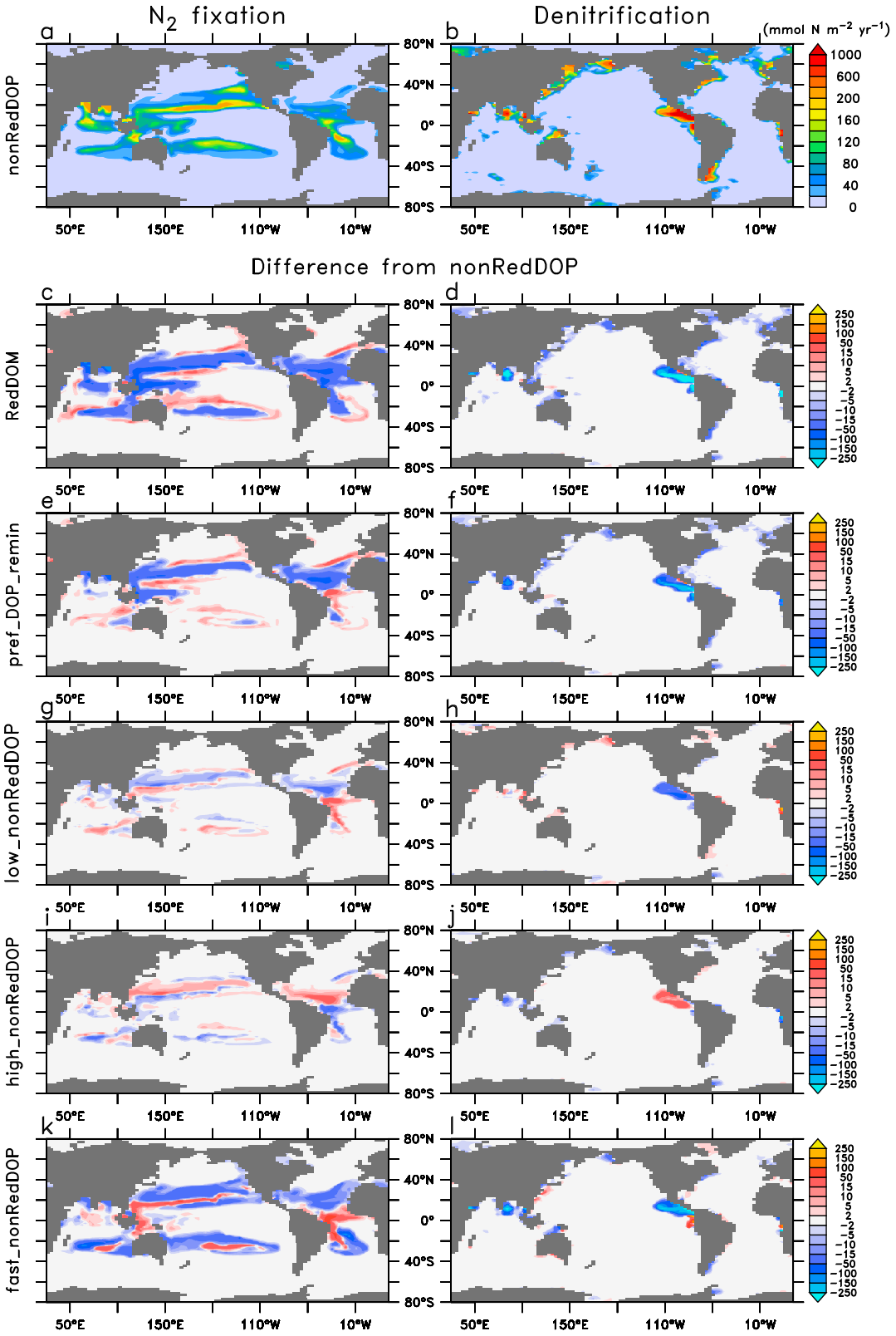

Figure 6. Annual vertically integrated N_2 fixation and denitrification rates from (a and b) preferential DOP remineralization and phytoplankton DOP uptake (nonRedDOP) and the difference from nonRedDOP (i.e., model experiment minus nonRedDOP) in the (c and d) Redfield DOM (RedDOM), (e and f) preferential DOP remineralization (pref_DOP_remin), (g and h) non-Redfield DOP with low DOM production (low_nonRedDOP), (i and j) non-Redfield DOP with high DOM production (high_nonRedDOP), and (k and l) fast recycling non-Redfield DOP (fast_nonRedDOP).

Therefore, this reduction of export production and wc-denitrification (Table 3 and Figure 5c) is due to unrealistic DOM cycling, emphasizing the importance of having an observational constraint for simulating DON.

4. Conclusions

The large sensitivity of N_2 fixation and the size of the marine fixed-N inventory to variations in the stoichiometry of DOM dynamics in our model simulations raise questions about whether DOM schemes in the current generation of global climate-biogeochemical models are adequate to evaluate environmental controls on N_2 fixation, the marine fixed-N inventory, and marine productivity. Observed DON:DOP typically exceeds the canonical Redfield ratio (Figure 4b and Table 2), and thus, DOP will be overestimated in simple DOM schemes that assume a strict stoichiometric Redfield ratio. Such models will cause an overestimation of PO_4 limitation that reduces the ecological niche for typical model diazotrophs and may cause models with Redfield DOP dynamics to underestimate N_2 fixation. According to our model simulations, changes in the assumptions about non-Redfield DON:DOP dynamics alone can alter the global marine fixed-N budget and inventory by 4.7%, which suggests that models without non-Redfield DON:DOP dynamics may incorrectly predict future changes to N_2 fixation, the marine fixed-N inventory, and productivity.

Our model-data analysis suggests that surface DON is more recalcitrant than previously assumed in global climate-biogeochemical models that include only semilabile DOM which assume that the majority of DON remineralizes in the surface ocean. Our estimate is generally consistent with recent data assimilation studies that estimate that SR-DON has a lifetime of ~1–2 decades in the euphotic zone [*Letscher et al.*, 2013, 2015]. Only our simulations that assume that DON recycles back to NO_3 with these slower semirecalcitrant remineralization rates are capable of reproducing observed lateral surface DON gradients. This suggests that models that only include faster recycling semilabile DOM (i.e., lifetime less than a decade) [e.g., *Landolfi et al.*, 2013] will underestimate DON, N limitation, and N_2 fixation in the subtropical oligotrophic ocean.

Our best non-Redfield DOP model simulation (nonRedDOP) required both preferential DOP remineralization and phytoplankton DOP uptake to reproduce the observed patterns of DOP in the global surface ocean. Due to the increased P availability from the relatively labile DOP pool in the non-Redfield DOP model configuration, the ecological niche for diazotrophs expanded into the otherwise oligotrophic tropical/subtropical ocean gyres. This non-Redfield DOP simulation predicts an additional 30 Tg N yr^{-1} N_2 fixation that increased the size of the marine fixed-N inventory by 4.7% in the nonRedDOP simulation compared to the simulation with often-assumed Redfield DOM cycling that underestimates the observed fixed-N inventory (Table 3 and Figure 5).

The additional 8 Tg N yr^{-1} of N_2 fixation stimulated in the Atlantic Ocean is primarily responsible the increase in the size of the marine fixed-N inventory due to its large spatial separation from suboxic zones. Whereas in the Pacific, additional N_2 fixation near suboxic zones stimulated additional productivity and even more wc-denitrification, which prevented a surplus to the marine fixed-N budget there. This highlights the importance of considering a dynamic N_2-fixation-denitrification feedbacks and further illustrates the hypothesized importance of spatial separation between N_2 fixation and wc-denitrification to maintain the observed marine fixed-N inventory [*Landolfi et al.*, 2013]. Our results indicate a strong influence of non-Redfield DOP dynamics on surface nutrient cycling, the distribution of N_2 fixation, and the size of the marine fixed-N inventory and highlight the need for better global data sets of DON and DOP that can constrain more sophisticated DOM models to better quantify their importance on ocean biogeochemistry.

Appendix A: Marine Ecosystem-Biogeochemical Model Equations

The marine ecosystem-biogeochemical model used here is a modified version of *Somes et al.* [2013] that includes improvements to the marine ecosystem model outlined in *Keller et al.* [2012] and the implementation of dissolved organic matter (see section 2.2). Here we provide a description of the model equations and parameters (Table A1) used in this study and refer to the previous studies referenced above for a complete model description and evaluation. Figure A1 shows the basin scale comparison with phosphate, dissolved oxygen, dissolved inorganic carbon, and carbon 14 observations.

Table A1. Marine Ecosystem-Biogeochemical Parameters

Parameter	Symbol	Value	Units
Phytoplankton (P_O, P_D) Coefficients			
Initial slope of P-I curve	α	0.1	$(\mathrm{W\,m^{-2}})^{-1}\,\mathrm{d^{-1}}$
Photosynthetically active radiation	PAR	0.43	-
Light attenuation in water	k_w	0.04	$\mathrm{m^{-1}}$
Light attenuation through phytoplankton	k_c	0.03	$\mathrm{m^{-1}(mmol\,m^{-3})^{-1}}$
Light attenuation through sea ice	k_i	5	$\mathrm{m^{-1}}$
NO_3 uptake half saturation	k_{NO3}	0.7	$\mathrm{mmol\,m^{-3}}$
PO_4 uptake half saturation	k_{PO4}	0.04375	$\mathrm{mmol\,m^{-3}}$
Fe uptake half saturation	k_{Fe}	0.12	$\mathrm{nmol\,m^{-3}}$
Maximum growth rate (at 0°C)	a_0	0.6	$\mathrm{d^{-1}}$
Phytoplankton fast-recycling rate (at 0°C)	μ_{P_O0}	0.015	$\mathrm{d^{-1}}$
Phytoplankton specific mortality rate	m_{P_O}	0.03	$\mathrm{d^{-1}}$
Diazotrophs' growth handicap	h_{P_D}	0.08	-
Diazotroph fast-recycling rate (at 0°C)	$\mu_{P_{D0}}$	0.001	$\mathrm{d^{-1}}$
Zooplankton (Z) Coefficients			
Assimilation efficiency	γ	0.7	
Maximum grazing rate (at 0°C)	gZ	0.4	$\mathrm{d^{-1}}$
Growth efficiency	ϖ	0.57	
Mortality	mz	0.06	$\mathrm{d^{-1}}$
Grazing preference P_O	ψ_{P_O}	0.3	
Grazing preference P_D	ψ_{P_D}	0.1	
Grazing preference Z	ψ_Z	0.3	
Grazing preference D	ψ_D	0.3	
Grazing half saturation	k_{graz}	0.15	$\mathrm{mmol\,N\,m^{-3}}$
Detritus (D) Coefficients			
Remineralization rate	μ_{D0}	0.07	$\mathrm{d^{-1}}$
Sinking speed at surface	w_{D0}	16	$\mathrm{m\,d^{-1}}$
Increase of sinking speed with depth	m_w	0.06	$\mathrm{d^{-1}}$
e-folding temperature of biological rates	T_b	15.65	°C
Elemental Ratios			
Molar oxygen:nitrogen	$R_{O:N}$	10.0	
Molar carbon:nitrogen	$R_{C:N}$	6.625	
Phytoplankton nitrogen:phosphorus	$R_{N:P_{P_O}}$	16	
Diazotroph nitrogen:phosphorus	$R_{N:P_{PD}}$	28	
Diazotroph nitrogen:phosphorus	$R_{N:P_{PD}}$	16	
Zooplankton nitrogen:phosphorus	$R_{N:P_Z}$	16	

The growth rate for ordinary phytoplankton (J_O) and diazotrophs (J_D) are

$$J^*_{P_O} = J^{\max}_{P_O} \min\left\{ \frac{\alpha I}{\left[J^{\max 2}_{P_O} + (\alpha I)^2\right]^{1/2}}, \frac{\mathrm{NO_3}}{k_{\mathrm{DIN}} + \mathrm{NO_3}}, \max\left(\frac{\mathrm{PO_4^{3-}}}{k_{\mathrm{PO_4^{3-}}} + \mathrm{PO_4^{3-}}}, h_{\mathrm{DOP}} \frac{\mathrm{DOP}}{k_{\mathrm{PO_4^{3-}}} + \mathrm{DOP}} \right) \right\} \tag{A1}$$

$$J^*_{P_D} = h_{P_D} J^{\max}_{P_O} \min\left\{ \frac{\alpha I}{\left[h_{P_D} J^{\max 2}_{P_O} + (\alpha I)^2\right]^{1/2}}, \max\left(\frac{\mathrm{PO_4^{3-}}}{k_{\mathrm{PO_4^{3-}}} + \mathrm{PO_4^{3-}}}, h_{\mathrm{DOP}} \frac{\mathrm{DOP}}{k_{\mathrm{PO_4^{3-}}} + \mathrm{DOP}} \right) \right\}, \tag{A2}$$

where the maximum growth rate $J_{PO}{}^{\max} = a_0(\mathrm{Fe}/(k_{\mathrm{Fe}} + \mathrm{Fe}))\exp(T/T_b)$, I is the shortwave solar insolation, k_{Fe} is the iron uptake half saturation, and monthly dissolved iron is calculated by the BLING biogeochemical model [*Galbraith et al.*, 2010] , which determines iron limitation in the our model (Figure A2). The grazing rate on each type of prey is

$$G^*_{P_O} = g^{*\max}_Z Z \frac{\psi_{P_O}}{\phi} P_O \tag{A3}$$

$$G^*_{PD} = g^{*\max}_Z Z \frac{\psi_{P_D}}{\phi} P_D \tag{A4}$$

$$G^*_D = g^{*\max}_Z Z \frac{\psi_D}{\varphi} D \tag{A5}$$

$$G^*_Z = g^{*\max}_Z Z \frac{\psi_Z}{\phi} Z^2, \tag{A6}$$

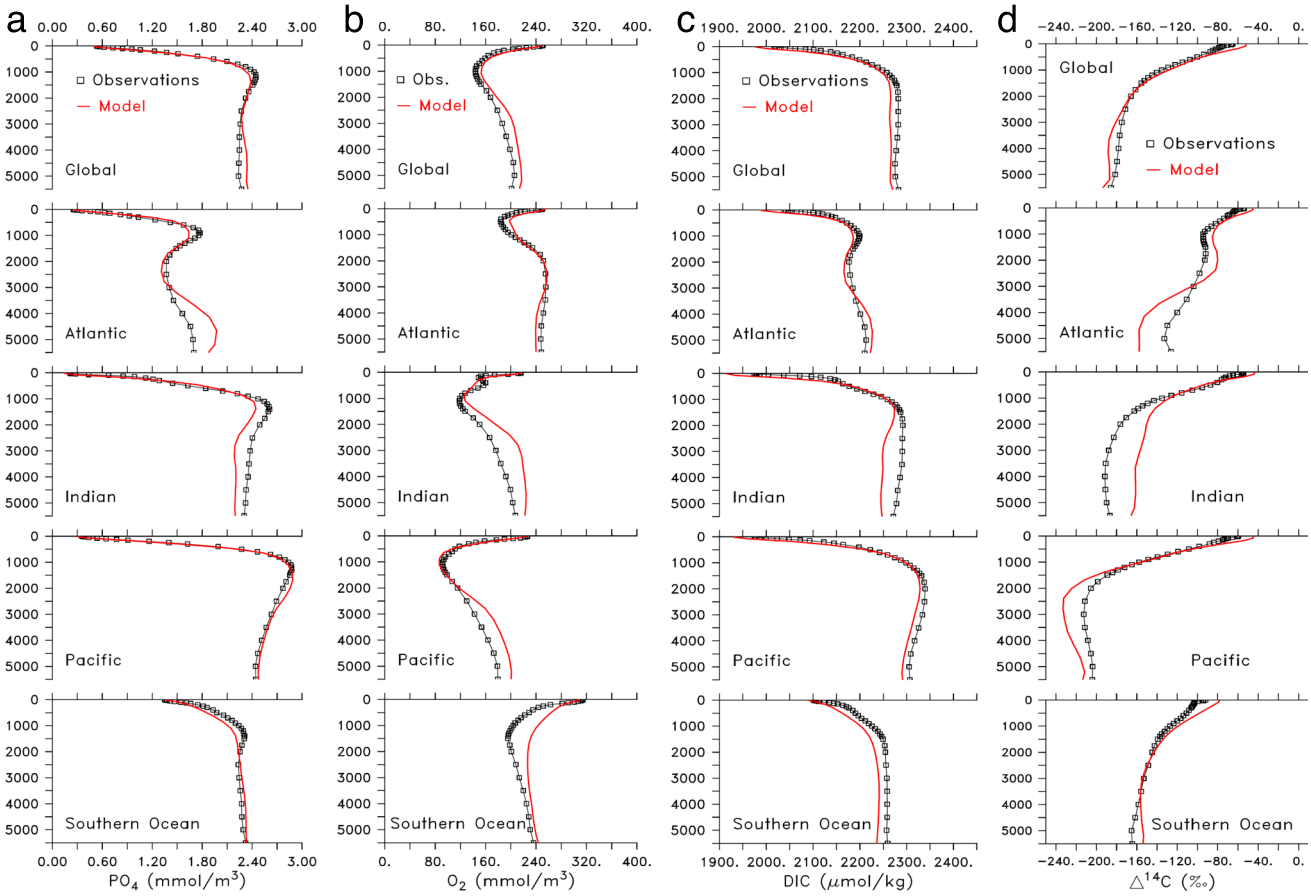

Figure A1. Annual basin-scale model-data comparison of (a) phosphate, (b) dissolved oxygen, (c) dissolved inorganic carbon, and (d) carbon-14 from the nonRedDOP experiment with Global Data Analysis Project [*Key et al.*, 2004] and World Ocean Atlas 2009 [*Garcia et al.*, 2010a, 2010b] observations.

where

$$g_Z^{*\max} = g_Z \max\left\{0, [0.5(\tanh(O_2 - 8) + 1)] b^{c\min(20,T)}\right\} \tag{A7}$$

and $\Phi = P_O + P_D + D + Z + K_G$ with temperature T in degrees Celsius.

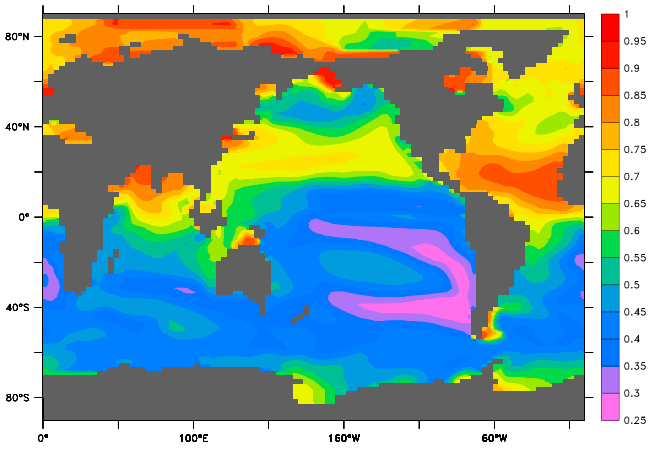

Figure A2. Annual iron limitation mask applied to phytoplankton maximum growth rate based on monthly surface dissolved iron concentrations from the BLING model [*Galbraith et al.*, 2010]. See Appendix A for further description.

Detritus is generated from sloppy zooplankton feeding and mortality among the three classes of plankton and is the only component of the ecosystem model to sink. It does so at a speed of

$$w_D = \left\{ \begin{array}{l} w_{D0} + m_w z, \;\; z \le 1000\,\mathrm{m} \\ w_{D0} + m_w 1000\,\mathrm{m}, \, z \le 1000\,\mathrm{m} \end{array} \right\}, \tag{A8}$$

increasing linearly with depth z from $w_{D0} = 16\,\mathrm{m\,d^{-1}}$ at the surface to $76\,\mathrm{m\,d^{-1}}$ at 1 km depth and constant below that, generally consistent with observations [*Berelson*, 2001]. The remineralization rate of detritus is temperature dependent and decreases by a factor of 5 in oxygen deficient waters, as O_2 decreases from 10 μm to 0 μm:

$$\mu_D = \mu_{D0} \exp\left(T/Tb\right)[0.75 + 0.25\tanh(O_2 - 6)]. \tag{A9}$$

Remineralization transforms the N and P content of detritus to NO_3 and PO_4. Photosynthesis produces oxygen, while respiration consumes oxygen, at rates equal to the consumption and remineralization rates of PO_4, respectively, multiplied by the constant ratio $R_{O:P}$. Dissolved oxygen exchanges with the atmosphere in the surface layer (F_{sfc}) according to the Ocean Carbon-Cycle Model Intercomparison Project protocol [*Orr et al.*, 2001].

Oxygen consumption in oxygen deficient waters ($O_2 < \sim 7$ μm) is inhibited, according to

$$r_{\mathrm{sox}}^{O_2} = 0.5[\tanh(O_2 - 3) + 1] \tag{A10}$$

but is replaced by the oxygen-equivalent oxidation of nitrate,

$$r_{\mathrm{sox}}^{NO_3^-} = 0.5[1 - \tanh(O_2 - 3)]. \tag{A11}$$

Denitrification consumes nitrate at a rate of 80% of the oxygen equivalent rate, as NO_3 is a more efficient oxidant on a mol per mol basis (i.e., 1 mol of NO_3 can accept $5\,e^-$, while 1 mol of O_2 can accept only $4\,e^-$).

We include the ben-denitrification scheme that parameterizes ben-denitrification based on the rain ratio of carbon flux (RR_{POC}; $\mathrm{mmol\,C\,m^{-2}\,d^{-1}}$) into the sediments and bottom water oxygen and nitrate (μm) [*Bohlen et al.*, 2012]:

$$BenDen = \left(0.09872 + 0.22944 \times 0.9811^{bwO_2 - bwNO_3}\right) \tag{A12}$$

BenDen is the rate ($\mathrm{mmol\,N\,m^{-2}\,d^{-1}}$) at which nitrate is removed from the bottom water. We assume that the rain rate of carbon into the sediments occurs at a ratio of $R_{C:N} = 6.625$ of the nitrogen in the sinking organic detritus. Since the continental shelves are not well resolved in the model, we use an additional subgrid-scale parameterization according to high-resolution bathymetry [see *Somes et al.*, 2010b].

The full set of prognostic marine ecosystem-biogeochemical equations are as follows:

$$\frac{\partial PO_4^{3-}}{\partial t} = \lambda_{DOP} DOP + \left[\mu_D^* D + \gamma(1-\varpi)\left(G_{P_D}^* \frac{R_{N:P_Z}}{R_{N:P_{P_D}}} + G_{P_O}^* + G_Z^* + G_D^* \right) \right.$$
$$\left. + (1 - \sigma 2_{DOM}) \mu_{P_O}^* P_O - \left(1 - u_{DOP_{P_O}}\right) J_O^* P_O \right] R_{P:N_{P_O}} - \left(1 - u_{DOP_{P_D}}\right) J_D^* P_D \subset R_{P:N_{P_D}} \tag{A13}$$

$$\frac{\partial \mathrm{NO_3}}{\partial t} = \left[\lambda_{\mathrm{DON}} \mathrm{DON} + \mu_D^* D + \gamma(1-\varpi)\left(G_{P_D}^* \frac{R_{N:P_Z}}{R_{N:P_{P_D}}} + G_{P_O}^* + G_Z^* + G_D^* \right) + G_{P_D}^* \left(1 - \frac{R_{N:P_Z}}{R_{N:P_{P_D}}}\right) \right. \tag{A14}$$
$$\left. + (1 - \sigma 2_{\mathrm{DOM}}) \mu_{P_O}^* P_O - J_O^* P_O - u_N J_D^* P_D \right] \times \left[1 - 0.8 R_{O:N} r_{\mathrm{sox}}^{NO_3^-}\right] - BenDen$$

$$\frac{\partial \mathrm{DOP}}{\partial t} = \left(\sigma 1_{\mathrm{DOM}} \upsilon_{P_O} P_O + \sigma 2_{\mathrm{DOM}} \mu_{P_O}^* \mathrm{PO} - \mu_{\mathrm{DOP}_{P_O}} J_O^* P_O\right) R_{P:N_{P_O}} - u_{\mathrm{DOP}_{P_D}} J_D^* P_D R_{P:N_{P_D}} - \lambda_{\mathrm{DOP}}^* \mathrm{DOP} \tag{A15}$$

$$\frac{\partial \mathrm{DON}}{\partial t} = \sigma 1_{\mathrm{DOM}} \upsilon_{P_O} + \sigma 2_{\mathrm{DOM}} \mu_{P_O}^* P_O - \lambda_{\mathrm{DON}}^* \mathrm{DON} \tag{A16}$$

$$\frac{\partial P_O}{\partial t} = J_O^* P_O - \mu_{P_O}^* P_O - \upsilon_{P_O} P_O - G_{P_O}^* Z \tag{A17}$$

$$\frac{\partial P_D}{\partial t} = J_D^* P_D - \mu_{P_D}^* P_D - G_{P_D}^* Z \tag{A18}$$

$$\frac{\partial Z}{\partial t} = \gamma \varpi \left(G_{P_O}^* + G_{P_D}^* + G_Z^* + G_D^* \right) Z - (1 - \gamma\varpi) G_Z^* Z - \upsilon_Z Z^2 \tag{A19}$$

$$\frac{\partial D}{\partial t} = (1-\gamma)\left(G_{P_O}^* + G_{P_D}^* + G_Z^* + G_D^* \right) Z + (1 - \sigma 1_{\mathrm{DOM}}) \upsilon_{P_O} P_O + \upsilon_Z Z^2 - \mu_D^* D - G_D^* Z - w_D \frac{\partial D}{\partial z} \tag{A20}$$

Acknowledgments
We thank three anonymous reviewers for their constructive comments that significantly improved the paper. Angela Landolfi and Andreas Schmittner also provided helpful comments. We thank the U.S. Global Ocean Carbon and Repeat Hydrography (http://ushydro.ucsd.edu/) program and the Atlantic Meridional Transect Consortium (http://www.bodc.ac.uk/projects/uk/amt/) including George Wolff (wolff@liverpool.ac.uk) for making their dissolved organic matter data available. This study was supported by the Deutsche Forschungsgemeinschaft via the Sonderforschungbereich 754 "Climate-Biogeochemistry Interactions in the Tropical Ocean."

References

Abell, J., S. Emerson, and P. Renaud (2000), Distributions of TOP, TON and TOC in the North Pacific subtropical gyre: Implications for nutrient supply in the surface ocean and remineralization in the upper thermocline, *J. Mar. Res.*, *58*, 203–222.

Antoine, D., J. André, and A. Morel (1996), Oceanic primary production: 2. Estimation at global scale from satellite (coastal zone color scanner) chlorophyll, *Global Biogeochem. Cycles*, *10*(1), 57–69.

Aumont, O., E. Maier-Reimer, S. Blain, and P. Monfray (2003), An ecosystem model of the global ocean including Fe, Si, P colimitations, *Global Biogeochem. Cycles*, *17*(2), 1060, doi:10.1029/2001GB001745.

Benner, R. (2002), Chemical composition and reactivity, in *Biogeochemistry of Marine Dissolved Oragnic Matter*, edited by D. A. Hansell and C. A. Carlson, pp. 59–90, Academic Press, San Diego, Calif.

Berelson, W. M. (2001), Particle settling rates increase with depth in the ocean, *Deep Sea Res., Part II*, *49*(1–3), 237–251.

Berman, T., and D. Bronk (2003), Dissolved organic nitrogen: A dynamic participant in aquatic ecosystems, *Aquat. Microb. Ecol.*, *31*(1981), 279–305.

Bianchi, D., J. P. Dunne, J. L. Sarmiento, and E. D. Galbraith (2012), Data-based estimates of suboxia, denitrification, and N_2O production in the ocean and their sensitivities to dissolved O_2, *Global Biogeochem. Cycles*, *26*, GB2009, doi:10.1029/2011GB004209.

Bohlen, L., A. W. Dale, and K. Wallmann (2012), Simple transfer functions for calculating benthic fixed nitrogen losses and C:N:P regeneration ratios in global biogeochemical models, *Global Biogeochem. Cycles*, *26*, GB3029, doi:10.1029/2011GB004198.

Breitbarth, E., A. Oschlies, and J. LaRoche (2007), Physiological constraints on the global distribution of Trichodesmium—Effect of temperature on diazotrophy, *Biogeosciences*, *4*, 53–61.

Bronk, D. A., J. H. See, P. Bradley, and L. Killberg (2007), DON as a source of bioavailable nitrogen for phytoplankton, *Biogeosciences*, *4*(3), 283–296, doi:10.5194/bg-4-283-2007.

Church, M. J., H. W. Ducklow, and D. M. Karl (2002), Multiyear increases in dissolved organic matter inventories at Station ALOHA in the North Pacific subtropical gyre, *Limnol. Oceanogr.*, *47*(1), 1–10, doi:10.4319/lo.2002.47.1.0001.

Clark, L. L., E. D. Ingall, and R. Benner (1998), Marine phosphorus is selectively remineralized, *Nature*, *393*, 426, doi:10.1038/30881.

Codispoti, L. A., and J. P. Christensen (1985), Nitrification, denitrification and nitrous oxide cycling in the eastern tropical South Pacific Ocean, *Mar. Chem.*, *16*(4), 277–300, doi:10.1016/0304-4203(85)90051-9.

Codispoti, L. A., J. A. Brandes, J. P. Christensen, A. H. Devol, S. W. A. Naqvi, H. W. Paerl, and T. Yoshinari (2001), The oceanic fixed nitrogen and nitrous oxide budgets: Moving targets as we enter the anthropocene?, *Sci. Mar.*, *65*, 85–105.

Cotner, J. B., Jr., and R. G. Wetzel (1992), Uptake of dissolved inorganic and organic phosphorus compounds by phytoplankton and bacterioplankton, *Limnol. Oceanogr.*, *37*(2), 232–243.

Deutsch, C., J. L. Sarmiento, D. M. Sigman, N. Gruber, and J. P. Dunne (2007), Spatial coupling of nitrogen inputs and losses in the ocean, *Nature*, *445*(7124), 163–167, doi:10.1038/nature05392.

DeVries, T., C. Deutsch, P. A. Rafter, and F. Primeau (2013), Marine denitrification rates determined from a global 3-D inverse model, *Biogeosciences*, *10*(4), 2481–2496, doi:10.5194/bg-10-2.

Dietze, H., and U. Loeptien (2013), Revisiting "nutrient trapping" in global coupled biogeochemical ocean circulation models, *Global Biogeochem. Cycles*, *27*, 265–284, doi:10.1002/gbc.20029.

Dutkiewicz, S., B. A. Ward, J. R. Scott, and M. J. Follows (2014), Understanding predicted shifts in diazotroph biogeography using resource competition theory, *Biogeosciences*, *11*(19), 5445–5461, doi:10.5194/bg-11-5445-2014.

Dyhrman, S. T., P. D. Chappell, S. T. Haley, J. W. Moffett, E. D. Orchard, J. B. Waterbury, and E. A. Webb (2006), Phosphonate utilization by the globally important marine diazotroph Trichodesmium, *Nature*, *439*(7072), 68–71, doi:10.1038/nature04203.

Eby, M., K. Zickfeld, A. Montenegro, D. Archer, K. J. Meissner, and A. J. Weaver (2009), Lifetime of anthropogenic climate change: Millennial time scales of potential CO_2 and surface temperature perturbations, *J. Clim.*, *22*(10), 2501–2511, doi:10.1175/2008jcli2554.1.

Eugster, O., and N. Gruber (2012), A probabilistic estimate of global marine N-fixation and denitrification, *Global Biogeochem. Cycles*, *26*, GB4013, doi:10.1029/2012GB004300.

Falkowski, P., E. Laws, R. Barber, and J. Murray (2003), Phytoplankton and their role in primary, new, and export production, in *Ocean Biogeochemistry SE-5*, edited by M. R. Fasham, pp. 99–121, Springer, Berlin.

Galbraith, E. D., A. Gnanadesikan, J. P. Dunne, and M. R. Hiscock (2010), Regional impacts of iron-light colimitation in a global biogeochemical model, *Biogeosciences*, *7*(3), 1043–1064, doi:10.5194/bg-7-1043-2010.

Garcia, H. E., R. A. Locarnini, T. P. Boyer, J. I. Antonov, M. M. Zweng, O. K. Baranov, and D. R. Johnson (2010a), *World Ocean Atlas 2009, Nutrients (Phosphate, Nitrate, Silicate)*, *NOAA Atlas NESDIS 70*, vol. 4, edited by S. Levitus, p. 398, U.S. Gov. Print. Off., Washington, D. C.

Garcia, H. E., R. A. Locarnini, T. P. Boyer, J. I. Antonov, O. K. Baranov, M. M. Zweng, D. R. Johnson, A. V. Mishonov, O. K. Baranova, and D. Seidov (2010b), *World Ocean Atlas 2009, Dissolved Oxygen, Apparent Oxygen Utilization, and Oxygen Saturation*, *NOAA Atlas NESDIS 70*, vol. 3, edited by S. Levitus, 184 pp., U.S. Gov. Print. Off., Washington, D. C.

Gent, P. R., and J. C. McWilliams (1990), Isopycnal mixing in ocean circulation models, *J. Phys. Oceanogr.*, *20*(1), 150–155, doi:10.1175/1520-0485(1990)020<0150:IMIOCM>2.0.CO;2.

Getzlaff, J., and H. Dietze (2013), Effects of increased isopycnal diffusivity mimicking the unresolved equatorial intermediate current system in an Earth System Climate Model, *Geophys. Res. Lett.*, *40*, 2166–2170, doi:10.1002/grl.50419.

Gregg, W. W. (2003), Ocean primary production and climate: Global decadal changes, *Geophys. Res. Lett.*, *30*(15), 1809, doi:10.1029/2003GL016889.

Großkopf, T., and J. Laroche (2012), Direct and indirect costs of dinitrogen fixation in Crocosphaera watsonii WH8501 and possible implications for the nitrogen cycle, *Front. Microbiol.*, *3*, 236, doi:10.3389/fmicb.2012.00236.

Großkopf, T., W. Mohr, T. Baustian, H. Schunck, D. Gill, M. M. M. Kuypers, G. Lavik, R. A. Schmitz, D. W. R. Wallace, and J. LaRoche (2012), Doubling of marine dinitrogen-fixation rates based on direct measurements, *Nature*, *488*(7411), 361–364, doi:10.1038/nature11338.

Gruber, N. (2008), The marine nitrogen cycle: Overview and challenges, in *Nitrogen in the Marine Environment*, 2nd ed., chap. 1, pp. 1–50, Academic Press, San Diego, Calif.

Hansell, D. A. (2013), Recalcitrant dissolved organic carbon fractions, *Annu. Rev. Mar. Sci.*, *5*, 421–445, doi:10.1146/annurev-marine-120710-100757.

Holl, C. M., and J. P. Montoya (2005), Interactions between nitrate uptake and nitrogen fixation in continuous cultures of the marine diazotroph Trichodesmium (Cyanobacteria), *J. Phycol.*, *41*(6), 1178–1183, doi:10.1111/j.1529-8817.2005.00146.x.

Ilyina, T., K. D. Six, J. Segschneider, E. Maier-Reimer, H. Li, I. Núñez-Riboni, and I. Nunez-Riboni (2013), Global ocean biogeochemistry model HAMOCC: Model architecture and performance as component of the MPI-Earth System Model in different CMIP5 experimental realizations, *J. Adv. Model. Earth Syst.*, *5*(2), 287–315, doi:10.1029/2012MS000178.

Kalnay, E., et al. (1996), The NCEP/NCAR 40-Year Reanalysis Project, *Bull. Am. Meteorol. Soc.*, *77*(3), 437–471, doi:10.1175/1520-0477(1996)077<0437:tnyrp>2.0.co;2.

Kalvelage, T., G. Lavik, P. Lam, S. Contreras, L. Arteaga, C. R. Loscher, A. Oschlies, A. Paulmier, L. Stramma, and M. M. M. Kuypers (2013), Nitrogen cycling driven by organic matter export in the South Pacific oxygen minimum zone, *Nat. Geosci.*, *6*, 228–234, doi:10.1038/ngeo1739.

Karl, D., A. Michaels, B. Bergman, D. Capone, E. Carpenter, R. Letelier, F. Lipschultz, H. Paerl, D. Sigman, and L. Stal (2002), Dinitrogen fixation in the world's oceans, *Biogeochemistry*, *57–58*(1), 47–98, doi:10.1023/a:1015798105851.

Karl, D. M., and K. M. Björkman (2002), Dynamics of DOP, in *Biogeochemistry of Marine Dissolved Organic Matter*, edited by D. M. Karl and C. A. Carlson, pp. 250–348, Academic Press, San Diego, Calif.

Karl, D. M., K. M. Björkman, J. E. Dore, L. Fujieki, D. V. Hebel, T. Houlihan, R. M. Letelier, and L. M. Tupas (2001), Ecological nitrogen-to-phosphorus stoichiometry at station ALOHA, *Deep Sea Res., Part II*, *48*(8–9), 1529–1566, doi:10.1016/S0967-0645(00)00152-1.

Keller, D. P., A. Oschlies, and M. Eby (2012), A new marine ecosystem model for the University of Victoria Earth System Climate Model, *Geosci. Model Dev.*, *5*(5), 1195–1220, doi:10.5194/gmd-5-1195-2012.

Key, R. M., A. Kozyr, C. L. Sabine, K. Lee, R. Wanninkhof, J. L. Bullister, R. A. Feely, F. J. Millero, C. Mordy, and T.-H. Peng (2004), A global ocean carbon climatology: Results from Global Data Analysis Project (GLODAP), *Global Biogeochem. Cycles*, *18*, GB4031, doi:10.1029/2004GB002247.

Koeve, W., and P. Kähler (2010), Heterotrophic denitrification vs. autotrophic anammox-quantifying collateral effects on the oceanic carbon cycle, *Biogeosciences*, *7*, 2327–2337, doi:10.5194/bg-7-2327-2010.

Krishnamurthy, A., J. K. Moore, N. Mahowald, C. Luo, S. C. Doney, K. Lindsay, and C. S. Zender (2009), Impacts of increasing anthropogenic soluble iron and nitrogen deposition on ocean biogeochemistry, *Global Biogeochem. Cycles*, *23*, GB3016, doi:10.1029/2008GB003440.

Kustka, A., S. Saudo-Wilhelmy, E. J. Carpenter, D. G. Capone, and J. A. Raven (2003), A revised estimate of the iron use efficiency of nitrogen fixation, with special reference to the marine cyanobacterium Trichodesmium spp. (Cyanophyta) 1, *J. Phycol.*, *39*(1), 12–25, doi:10.1046/j.1529-8817.2003.01156.x.

Lam, P., G. Lavik, M. M. Jensen, J. van de Vossenberg, M. Schmid, D. Woebken, D. Gutiérrez, R. Amann, M. S. M. Jetten, and M. M. M. Kuypers (2009), Revising the nitrogen cycle in the Peruvian oxygen minimum zone, *Proc. Natl. Acad. Sci. U.S.A.*, *106*(12), 4752–4757, doi:10.1073/pnas.0812444106.

Landolfi, A., H. Dietze, W. Koeve, and A. Oschlies (2013), Overlooked runaway feedback in the marine nitrogen cycle: The vicious cycle, *Biogeosciences*, *10*(3), 1351–1363, doi:10.5194/bg-10-1351-2013.

Large, W. G., G. Danabasoglu, J. C. McWilliams, P. R. Gent, and F. O. Bryan (2001), Equatorial circulation of a global ocean climate model with anisotropic horizontal viscosity, *J. Phys. Oceanogr.*, *31*(2), 518–536, doi:10.1175/1520-0485(2001)031<0518:ECOAGO>2.0.CO;2.

Le Quéré, C. L., et al. (2005), Ecosystem dynamics based on plankton functional types for global ocean biogeochemistry models, *Global Change Biol.*, *11*(11), 2016–2040, doi:10.1111/j.1365-2486.2005.1004.x.

Letelier, R., and D. Karl (1998), Trichodesmium spp. physiology and nutrient fluxes in the North Pacific subtropical gyre, *Aquat. Microb. Ecol.*, *15*(3), 265–276, doi:10.3354/ame015265.

Letscher, R. T., D. A. Hansell, C. A. Carlson, R. Lumpkin, and A. N. Knapp (2013), Dissolved organic nitrogen in the global surface ocean: Distribution and fate, *Global Biogeochem. Cycles*, *27*, 141–153, doi:10.1029/2012GB004449.

Letscher, R. T., J. K. Moore, Y.-C. Teng, and F. Primeau (2015), Variable C: N:P stoichiometry of dissolved organic matter cycling in the Community Earth System Model, *Biogeosciences*, *12*, 209–221.

Luo, Y.-W., et al. (2012), Database of diazotrophs in global ocean: Abundance, biomass and nitrogen fixation rates, *Earth Syst. Sci. Data*, *4*(1), 47–73, doi:10.5194/essd-4-47-2012.

Mahowald, N. M., et al. (2009), Atmospheric iron deposition: Global distribution, variability, and human perturbations, *Annu. Rev. Mar. Sci.*, *1*, 245–278.

Martiny, A. C., M. L. Coleman, and S. W. Chisholm (2006), Phosphate acquisition genes in Prochlorococcus ecotypes: Evidence for genome-wide adaptation, *Proc. Natl. Acad. Sci. U.S.A.*, *103*, 12,552–12,557, doi:10.1073/pnas.0601301103.

Mather, R. L., S. E. Reynolds, G. A. Wolff, R. G. Williams, S. Torres-Valdes, E. M. S. Woodward, A. Landolfi, X. Pan, R. Sanders, and E. P. Achterberg (2008), Phosphorus cycling in the North and South Atlantic Ocean subtropical gyres, *Nat. Geosci.*, *1*(7), 439–443, doi:10.1038/ngeo232.

Mills, M. M., C. Ridame, M. Davey, J. La Roche, and R. J. Geider (2004), Iron and phosphorus co-limit nitrogen fixation in the eastern tropical North Atlantic, *Nature*, *429*(6989), 292–294, doi:10.1038/nature02550.

Mohr, W., T. Großkopf, D. W. R. Wallace, and J. LaRoche (2010), Methodological underestimation of oceanic nitrogen fixation rates, *PLoS One*, *5*(9), e12583.

Monteiro, F. M., and M. J. Follows (2012), On nitrogen fixation and preferential remineralization of phosphorus, *Geophys. Res. Lett.*, *39*, L06607, doi:10.1029/2012GL050897.

Monteiro, F. M., S. Dutkiewicz, and M. J. Follows (2011), Biogeographical controls on the marine nitrogen fixers, *Global Biogeochem. Cycles*, *25*, GB2003, doi:10.1029/2010GB003902.

Moore, J. K., and S. C. Doney (2007), Iron availability limits the ocean nitrogen inventory stabilizing feedbacks between marine denitrification and nitrogen fixation, *Global Biogeochem. Cycles*, *21*, GB2001, doi:10.1029/2006GB002762.

Moore, L., M. Ostrowski, D. Scanlan, K. Feren, and T. Sweetsir (2005), Ecotypic variation in phosphorus-acquisition mechanisms within marine picocyanobacteria, *Aquat. Microb. Ecol.*, *39*, 257–269, doi:10.3354/ame039257.

Moore, M. C., et al. (2009), Large-scale distribution of Atlantic nitrogen fixation controlled by iron availability, *Nat. Geosci.*, *2*(12), 867–871, doi:10.1038/ngeo667.

Mulholland, M. R., K. Ohki, and D. G. Capone (2001), Nutrient controls on nitrogen uptake and metabolism by natural populations and cultures of Trichodesmium (Cyanobacteria), *J. Phycol.*, *37*(6), 1001–1009, doi:10.1046/j.1529-8817.2001.00080.x.

Najjar, G., J. L. Sarmiento, and J. R. Toggweiler (1992), Downward transport and fate of organic matter in the ocean: Simulations with a general circulation model, *Global Biogeochem. Cycles*, *6*(1), 45–76, doi:10.1029/91GB02718.

O'Neil, J. M. (1999), Grazer interactions with nitrogen-fixing marine cyanobacteria: Adaptation for N-acquisition?, *Bull. Inst. Oceanogr.*, (Spec. 19), 293–317.

Orr, J. C., et al. (2001), Estimates of anthropogenic carbon uptake from four three-dimensional global ocean models, *Global Biogeochem. Cycles*, *15*(1), 43–60, doi:10.1029/2000GB001273.

Pandey, K. D., S. P. Shukla, P. N. Shukla, D. D. Giri, J. S. Singh, P. Singh, and A. K. Kashyap (2004), Cyanobacteria in Antarctica: Ecology, physiology and cold adaptation, *Cell. Mol. Biol. (Noisy-le-grand)*, *50*(5), 575–584.

Paulmier, A., I. Kriest, and A. Oschlies (2009), Stoichiometries of remineralisation and denitrification in global biogeochemical ocean models, *Biogeosciences*, *6*(5), 923–935, doi:10.5194/bg-6-923-2009.

Peltier, W. R. (2004), Global glacial isostasy and the surface of the Ice-Age Earth: The Ice-5G (VM2) model and GRACE, *Annu. Rev. Earth Planet. Sci.*, *32*(1), 111–149, doi:10.1146/annurev.earth.32.082503.144359.

Redfield, A. C. (1958), The biological control of chemical factors in the environment, *Am. Sci.*, *46*(3), 205–221.

Richards, F. (1965), Anoxic basins and fjords, in *Chemical Oceanography*, edited by J. Riley and G. Skirrow, pp. 611–645, Academic Press, London.
Sannigrahi, P., E. D. Ingall, and R. Benner (2005), Cycling of dissolved and particulate organic matter at station Aloha: Insights from ^{13}C NMR spectroscopy coupled with elemental, isotopic and molecular analyses, *Deep Sea Res., Part I*, *52*, 1429–1444, doi:10.1016/j.dsr.2005.04.001.
Sanudo-Wilhelmy, S. A., A. B. Kustka, C. J. Gobler, D. A. Hutchins, M. Yang, K. Lwiza, J. Burns, D. G. Capone, J. A. Raven, and E. J. Carpenter (2001), Phosphorus limitation of nitrogen fixation by Trichodesmium in the central Atlantic Ocean, *Nature*, *411*(6833), 66–69, doi:10.1038/35075041.
Schmittner, A., A. Oschlies, X. Giraud, M. Eby, and H. L. Simmons (2005), A global model of the marine ecosystem for long-term simulations: Sensitivity to ocean mixing, buoyancy forcing, particle sinking, and dissolved organic matter cycling, *Global Biogeochem. Cycles*, *19*, GB3004, doi:10.1029/2004GB002283.
Simmons, H. L., S. R. Jayne, L. C. S. Laurent, and A. J. Weaver (2004), Tidally driven mixing in a numerical model of the ocean general circulation, *Ocean Modell.*, *6*(3–4), 245–263, doi:10.1016/S1463-5003(03)00011-8.
Sohm, J. A., and D. G. Capone (2006), Phosphorus dynamics of the tropical and subtropical north Atlantic: Trichodesmium spp. versus bulk plankton, *Mar. Ecol. Prog. Ser.*, *317*, 21–28, doi:10.3354/meps317021.
Sohm, J. A., and D. G. Capone (2010), Zonal differences in phosphorus pools, turnover and deficiency across the tropical North Atlantic Ocean, *Global Biogeochem. Cycles*, *24*, GB2008, doi:10.1029/2008GB003414.
Somes, C. J., A. Schmittner, and M. A. Altabet (2010a), Nitrogen isotope simulations show the importance of atmospheric iron deposition for nitrogen fixation across the Pacific Ocean, *Geophys. Res. Lett.*, *37*, L23605, doi:10.1029/2010GL044537.
Somes, C. J., A. Schmittner, E. D. Galbraith, M. F. Lehmann, M. A. Altabet, J. P. Montoya, R. M. Letelier, A. C. Mix, A. Bourbonnais, and M. Eby (2010b), Simulating the global distribution of nitrogen isotopes in the ocean, *Global Biogeochem. Cycles*, *24*, GB4019, doi:10.1029/2009GB003767.
Somes, C. J., A. Oschlies, and A. Schmittner (2013), Isotopic constraints on the pre-industrial oceanic nitrogen budget, *Biogeosciences*, *10*(9), 5889–5910, doi:10.5194/bg-10-5889-2013.
Thamdrup, B., and T. Dalsgaard (2002), Production of N(2) through anaerobic ammonium oxidation coupled to nitrate reduction in marine sediments, *Appl. Environ. Microbiol.*, *68*(3), 1312–1318, doi:10.1128/AEM.68.3.1312-1318.2002.
Vidal, M., C. Duarte, and S. Agusti (1999), Dissolved organic nitrogen and phosphorus pools and fluxes in the central Atlantic Ocean, *Limnol. Oceanogr.*, *44*(1), 106–115.
Vidal, M., C. Duarte, S. Agustí, J. Gasol, and D. Vaqué (2003), Alkaline phosphatase activities in the central Atlantic Ocean indicate large areas with phosphorus deficiency, *Mar. Ecol. Prog. Ser.*, *262*, 43–53, doi:10.3354/meps262043.
Weaver, A. J., et al. (2001), The UVic Earth System Climate Model: Model description, climatology, and applications to past, present and future climates, *Atmos. Ocean*, *39*(4), 361–428.
Weber, T., and C. Deutsch (2014), Local versus basin-scale limitation of marine nitrogen fixation, *Proc. Natl. Acad. Sci. U.S.A.*, *111*(24), 8741–8746, doi:10.1073/pnas.1317193111.
Wu, J. (2000), Phosphate depletion in the western North Atlantic Ocean, *Science*, *289*(5480), 759–762, doi:10.1126/science.289.5480.759.